frontiers | Frontiers in Mechanical Engineering

TYPE Review
PUBLISHED 28 July 2023
DOI 10.3389/fmech.2023.1087021

OPEN ACCESS

EDITED BY
Himanshu Sahasrabudhe,
Michigan State University, United States

REVIEWED BY
Jonathan Pegues,
Sandia National Laboratories,
United States
Panagiotis Stavropoulos,
University of Patras, Greece

*CORRESPONDENCE
Eric S. Elton,
elton2@llnl.gov

†These authors have contributed equally to this work

RECEIVED 01 November 2022
ACCEPTED 13 July 2023
PUBLISHED 28 July 2023

CITATION
Wu Z, Wilson-Heid AE, Griffiths RJ and Elton ES (2023), A review on experimentally observed mechanical and microstructural characteristics of interfaces in multi-material laser powder bed fusion.
Front. Mech. Eng 9:1087021.
doi: 10.3389/fmech.2023.1087021

A review on experimentally observed mechanical and microstructural characteristics of interfaces in multi-material laser powder bed fusion

Ziheng Wu†, Alexander E. Wilson-Heid†, R. Joey Griffiths† and Eric S. Elton*†

Lawrence Livermore National Laboratory, Livermore, CA, United States

Additive manufacturing (AM) is a revolutionary technology. One of the key AM categories, metal powder-based fusion processes, has many advantages compared to conventional methods for fabricating structural materials, such as permitting increased geometric complexity. While single material metal powder AM has advanced significantly in the past decade, multi-material AM is gradually attracting more attention owing to the recent breakthrough in multi-material feedstock delivery and the growing interest of fabricating functionally graded components. Multi-material AM offers an alternative route for applications that require location dependent material properties and high geometrical complexity. The AM community has invented several ways to achieve compositional gradients and discrete boundaries in two and three dimensions using mechanical spreading, nozzle-based, electrophotographic, and hybrid techniques. This article reviews the current state of laser powder bed fusion based multi-material AM of metals with focuses on the characteristics of the material interface as well as the properties and performance of the AM built functionally graded materials. We show the common challenges and issues related to material transitions, such as defects, segregation, phase separation, and the efficacy of some potential solutions including material and process optimizations. Additionally, this study evaluates the applicability and limitations of the existing testing standards and methods for measuring mechanical performance of functionally graded materials. Finally, we discuss mechanical testing development opportunities, which can help multi-material AM move towards higher technological maturity. In general, we find that the link between gradient microstructure and mechanical properties is not well understood or studied and suggest several mechanical tests that may better inform this knowledge gap.

KEYWORDS

multi-material additive manufacturing, functionally graded material, laser powder bed fusion, mechanical testing, interfacial characterization

1 Introduction

Metal additive manufacturing has become an important manufacturing technology due to flexibility and ability to rapidly produce complex geometries (Vafadar et al., 2021; Chowdhury et al., 2022). There are three commonly used metal AM methods; wire arc AM (WAAM), laser powder bed fusion (LPBF), and directed energy deposition (DED). All of these methods depend on melting solid feedstock (either wire or powder) to form individual layers and eventually build the final part. In WAAM, wire is melted in an electrical arc to build each layer (Raut and Taiwade, 2021). In DED, powder is injected into a laser beam to melt and continuously build the part (Svetlizky et al., 2021). In LPBF, metal powder is deposited on each layer, and then fused with a laser into the desired shape on each layer (Chowdhury et al., 2022). Recoating with powder between layers allows for the part to be built over many layers.

Recently, there has been extensive interest in creating functionally graded materials (Schneck et al., 2021; Wei and Li, 2021; Hasanov et al., 2022). Functionally graded materials seek to provide unique properties, such as high heat transfer, wear resistance, or strength to different locations on the final part (Naebe and Shirvanimoghaddam, 2016; Li et al., 2020). While conventional manufacturing techniques can create gradients in simple geometries such as those seen in traditional dissimilar material welding (Wang et al., 2016), additive manufacturing creates the possibility of creating geometrically complex functionally graded materials with gradients in multiple dimensions (Li et al., 2020; Schneck et al., 2021; Wei and Li, 2021).

The creation of functional material gradients in parts allows for parts to be designed with material properties varying across the part. This opens up a meso-scale design space, where meso-scale indicates properties larger than the material microstructure, but smaller than whole part scale (Yu et al., 2017; Garcia et al., 2018). For example, Garcia et al. (2018) showed that beam deflection can be minimized by varying the location of two different materials within a beam, even though the overall density of the beam remained constant.

In multi-material metal AM applications, meso-scale design allows for both traditional part properties (strength or density) to be varied, but also thermal, electrical, or chemical resistance properties (Estrin et al., 2021). For example, iron and nickel alloys have also been combined with the aim of fabricating rotating shafts with magnetic cores for new electric motor designs (Andreiev et al., 2021). The geometries allowed by LPBF fabrication would reduce eddy current and increase motor efficiency. Titanium and aluminum alloy bimetallic parts have been considered for corrosion resistance and light weighting in aerospace applications, while parts made from two different aluminum alloys (Bhaduri et al., 2019) or aluminum and steel (Nguyen et al., 2019) have been considered for strength and corrosion resistance in automotive applications. In biomedical applications, nickel-titanium parts have been considered for medical applications such as bone implants, where a shape memory nickel alloy would allow for constant pressure between the implant and the surrounding bone, while the titanium core would provide strength (Bartolomeu et al., 2020). Finally, copper and nickel or tungsten alloys have been built into parts with enhanced thermal resistance and cooling properties for use in rocket engines (Marques et al., 2022) and confinement walls of internal confinement fusion reactors (Tan et al., 2019; Wei et al., 2022).

While the application space of multi-material metal AM parts is growing, the ability to build, design, and model these parts requires a clear understanding of how the different metals bond to each other. The strength of the bond is likely dependent on both the material properties, as well as the joining process. In this article, we review recent progress on multi-material laser powder bed fusion (MMLPBF) parts and processes, with an emphasis on the layers where interfacial bonding between different metals occurs. We limit ourselves to the widely used LPBF process which resembles welding. Therefore, parallels can be drawn between the dissimilar material welding and the MMLPBF processes. Specifically, the bond formation process between two materials is similar in MMLPBF and dissimilar material welding. This suggests that many mechanical tests used to characterize the strength of a dissimilar material weld can be directly applied to MMLPBF parts.

This review begins with a general overview of the MMLPBF process and specifically of different methods to spread multiple powders on a powder bed. We then present an overview of common defects and microstructural features developed at the boundary between dissimilar metals. A review of how the interface structure impacts mechanical performance follows. Finally, we review relevant mechanical tests from other methods for joining dissimilar materials, with the goal of suggesting tests that can give greater insight into how process and materials impact overall mechanical performance of the part. The goal of this review is to provide insight into prevalent microstructural properties and mechanical tests used in MMLPBF parts. As the link between these two is often unexplored, we suggest several mechanical tests that have been used outside of the LPBF community and may be applicable for further exploration of the link between microstructure and mechanical properties.

Beyond the general structure outlined above, we discuss relevant literature by material pairing. This potentially permits the discovery of correlations between microstructural features and mechanical testing data. While we attempted to correlate references with microstructural properties and mechanical testing data, we found very few references that contained both types of data. Thus, while the sections on microstructural features and mechanical testing are both organized by material pairing, by necessity they contain many unique references.

Finally, while this review does not include an extensive discussion on MMLPBF simulations, we note a few areas of interest here. First, the thermal gradient in the powder bed caused by multiple materials has been modeled by Foteinopoulos et al. (2020), who found that variations in the thermal field yielded different internal stress and deformation within the multi-material parts. Similarly, Mukherjee et al. (2018) modeled the residual stress of multi-material joints and found that the stress could be significantly lowered when using graded joints. Second, defects and porosity have also been studied computationally. Sun et al. (2020) found that variations in thermal conductivity and melt temperature could lead to high thermal gradients and a zone where Invar36 particles were surrounded by solidified Cu10Sn. Gu et al. (2021) used DEM-CFD modelling to study both powder spreading and process parameters and found that differences in thermal conductivity between Invar36 and Cu10Sn powder

TABLE 1 An overview of methods used to spread multiple metal powders for MMLPBF processes.

Spreading method	Advantages	Disadvantages	Citations
Dual hopper	Ease of implementation	Only 1D gradients possible	Sing et al. (2015)
			Scaramuccia et al. (2020)
			Wei et al. (2022)
Vibrating nozzle	Good resolution	Fixed gradient length	Al-Jamal et al. (2008)
		Slow speed compared to spreader bars	Wei et al. (2019a)
Vibrating nozzle with vacuum step	Resolution not limited by nozzle diameter	Fixed gradient length	Anstaett and Seidel (2016)
	Potentially faster than just vibrating nozzles	Slow speed compared to spreader bars	Girnth et al. (2019)
			Wei et al. (2019b)
			Wei et al. (2021)
			Walker et al. (2022)
Electrophotographic	High speed compared to nozzle systems	Electrophotographic plate fouling	Foerster et al. (2022a)
	Well studied physics		
Electrostatic	Ease of implementation	Low resolution	Elton et al. (2023)
	Arbitrary gradient length		
Charged drum and air pressure	High resolution	Fixed gradient length	Vialva, (2019)
			Aerosint - Multi-Material 3D Printing (2022)

variations in the melt pool depth and subsequently lack of fusion defects and general porosity as the Cu10Sn content increased. Third, microstructural modeling of multi-material joints has been carried out largely using CALculation of PHase Diagrams (CALPHAD) techniques. For example, Bobbio et al. (2018) utilized CALPHAD to suggest the addition of vanadium to avoid intermetallics in a Ti64/SS305L joint. However, the formation of an Fe-V intermetallic lead to cracking in a portion of the graded part. More complicated models that take into account rapid solidification seen during LPBF processes have also been proposed (Liu et al., 2020; Moustafa et al., 2020). For more in-depth reviews on MMLPBF simulations, we recommend the recent reviews by Stavropoulos and Foteinopoulos (2018), Ghanavati and Naffakh-Moosavy (2021), and Li et al. (2022).

2 Overview of MMLPBF processes

We begin with a broad overview of the laser powder bed fusion process, and how multiple materials are implemented into the traditional LPBF process. LPBF consists of spreading a thin layer of metal powder, which is then fused into the desired 2D shape using a laser. For metals, this involves melting the powder particles to form a solid part. The process then repeats, and a new layer of powder is spread and fused, until the entire part is built. Since the part is built layer-by-layer, the value of metal AM is in the unique geometries that can only be produced via additive and not subtractive processes (Schneck et al., 2021; Vafadar et al., 2021; Wei and Li, 2021).

Most LPBF machines are equipped to deposit a single material on each layer, typically by pushing or rolling the powder over the build area. To deposit multiple materials, machines must be equipped with a method to deposit multiple materials. Figure 1 schematically shows the common multi-material deposition techniques that have been implemented into LPBF machines. This section gives an overview of these techniques, and key findings are summarized in Table 1.

The simplest method spread multiple powders is to place two or more hoppers in the machine, and then selectively deposit powder from either hopper on different layers (Figure 1A) (Sing et al., 2015; Wei et al., 2022). By doing so, a one-dimensional gradient can be achieved in the final part. While careful control can produce extended one-dimensional gradients (Scaramuccia et al., 2020), it is difficult to produce 2D patterns using this method.

To produce gradients in 2 or 3 dimensions (i.e., XY or XYZ gradients, where X and Y are dimensions on the build plate area, and Z is in the height of the build volume), powder must be selectively deposited in specific areas of the build volume. One method to achieve this is to deposit powder through a vibrating nozzle. When vibration is applied to the nozzle, powder flows onto the build plate and the nozzle is translated to deposit powder in selected areas (Figure 1B) (Al-Jamal et al., 2008; Wei et al., 2019a). When no vibration is applied, cohesive forces keep the powder stationary in the nozzle. Multiple nozzles can be used to deposit multiple powders.

Similarly, a nozzle connected to a vacuum device can be used to remove powder from selected areas of the build volume (Figure 1C) (Anstaett and Seidel, 2016; Wei et al., 2018). The evacuated areas can then be refilled either using a vibrating nozzle or with a spreader bar pushing powder over the entire build area (Anstaett and Seidel, 2016; Wei et al., 2018; 2019b; 2021; Walker et al., 2022). Various other combinations of spreader bars, depositing nozzles, and suction nozzles have also been utilized (Girnth et al., 2019). While any

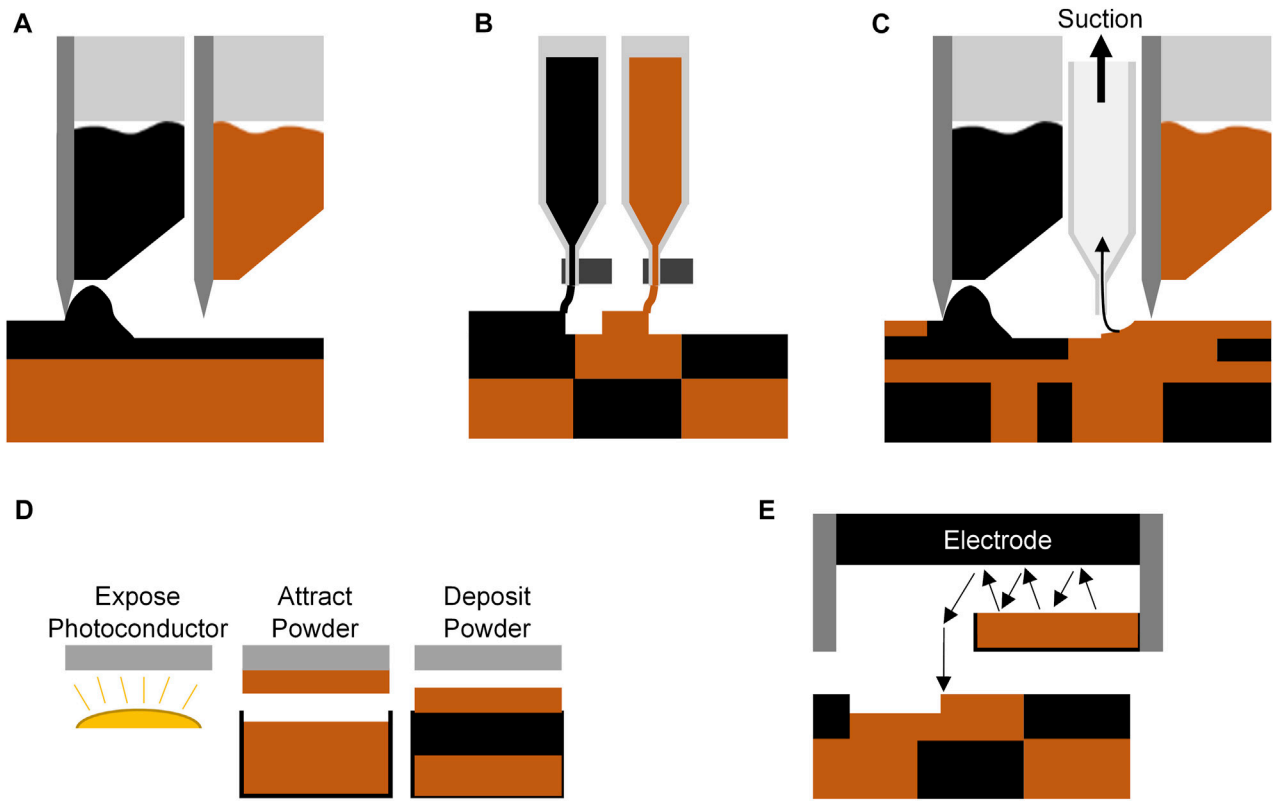

FIGURE 1
Schematics of powder deposition methods for multi-material LPBF processes. **(A)** Powder is deposited by two separate hoppers and blade systems. One powder is deposited per layer. **(B)** Multiple powders flow through vibrating nozzles to deposit multiple powders on each layer. **(C)** Hybrid system where powder is deposited via spreader blade, removed in certain locations with a suction nozzle, and refilled with a different powder via a spreader blade. **(D)** Main steps in the electrophotographic method of powder deposition. **(E)** Schematic of an electrostatic powder spreader that can deposit multiple powders per layer.

powder deposition method with a nozzle is slower than spreading with a spreader bar, the use of nozzles allows for 2D gradients to be placed on each layer. By varying the pattern on each layer, three dimensional gradients can be created. However, layer height homogeneity can degrade with nozzle based deposition systems, leading to defects in the printed part (Wei et al., 2019a).

There is also an emerging class of powder deposition techniques based on electrostatics that can produce gradients in 2 and 3 dimensions (Foerster et al., 2022a; Elton et al., 2023). While the use of electric fields to move conducting metal powders has found wide application in laser printers and xerography (Weigl, 1977), the application of this technology to metal additive manufacturing is relatively new. The most common of these techniques uses a photoconducting plate to transport powder from the hopper to the build area (Figure 1D) (Foerster et al., 2022a; 2022b). The photoconducting plate is charged in selected areas by exposing it to light, and powder is attracted to these areas. Once over the build area, an electric field is applied behind the plate to drive the powder onto the build area. The process can be repeated with multiple powders to create patterns on the build plate.

A similar technique, electrostatic powder spreading, utilizes a counter electrode located above a grounded powder hopper (Elton et al., 2023). When a high voltage is applied to the counter electrode, powder particles electrophoretically move between the hopper and counter electrode, where they eventually migrate over a mesh and fall onto the powder bed (Figure 1E). By having an array of electrodes, different materials can be deposited at different locations on the powder bed. Notably, by varying the applied voltage and spreader speed, the height of the deposited powder layer can be adjusted, suggesting that more gradual material gradients may be possible than those afforded by other techniques.

Finally, we make note of a hybrid electrostatic/nozzle based deposition method developed by Aerosint SA (Aerosint - Multi-Material 3D Printing, n.d.). This method uses a charged roller to pick up powder from a hopper. The powder is then blown off the roller using gas flow in selected areas (Wei and Li, 2021). By having multiple rollers, patterned powder beds with 500 μm resolution are capable of being produced (Vialva, 2019).

The methods outlined in this section are to deposit powder onto the build area, which is just one step in the full LPBF process. While powder deposition strategies are important to create the desired material patterns, the final part properties are also determined through the laser process parameters and mixing of the two materials. The ability to control laser parameters (e.g., laser power or scan speed), as well as post-processing can also affect the final properties of this part. The remainder of this review focuses on common defects and mechanical properties that are seen at the interface between two materials during MMLPBF builds.

TABLE 2 Summary of multi-material laser powder bed fusion studies that include microstructural and defect observations. Materials are listed by their commonly known names.

Material 1	Material 2	Gradient direction	Phases	Defects observed	Reference
Pure Fe	Al-12Si	1D vertical - discrete	-	Cracking	Demir and Previtali (2017)
SS316L	In718	1D vertical - discrete	-	Lack of fusion	Yusuf et al. (2021)
SS316L	In718	1D vertical - discrete	-	Cracking, Interdendritic porosity	Hinojos et al. (2016)
Ti6Al4V	TiB_2	1D vertical - discrete	-	Cracking, Wettability related pores	Chen et al. (2019a)
SS316L or K220 Cu	Ti64	1D vertical - discrete	$L2_1$, amorphous phase, and Ti_2Cu		Tey et al. (2020)
SS316L	C18400 Cu	1D vertical - discrete	-		Liu et al. (2014)
300 Maraging steel	Cu	Powder on plate - discrete	-	Cracking, Lack of fusion	Tan et al. (2018)
SS316L	In718 or Cu10Sn	3D - gradient	-	Cracking, Pores due to low powder packing	Wei et al. (2018)
SS316L	Cu10Sn	3D - step	$Cu_{3.8}Ni$, Cu_9NiSn_3	Cracking, Lack of fusion	Wei et al. (2019b)
SS316L	Cu10Sn	1D vertical - discrete	-	LME Cracking	Chen et al. (2020b)
SS316L	C52400 Cu	1D vertical - dual discrete	-	Cracking in SS316L, Pores	Bai et al. (2020)
H13	Cu	3D - discrete	-	Cracking	Al-Jamal et al. (2008)
Tool steel 1.2709	CuCr1Zr	3D - discrete	-	Cracking in steel	Anstaett et al. (2017)
18Ni300 Maraging steel	CuSn	1D vertical - discrete	-		Zhang et al. (2019)
Ti64	Invar 36	1D vertical - gradient	FeTi (B2), Fe_2Ti (Laves), Ni_3Ti (DO24), and $NiTi_2$	Cracking, Overflow	Bobbio et al. (2017)
Ti64	TiAl	1D vertical - discrete	-	-	Ge et al. (2015)
Ti6Al4V	Ti5Al2.5Sn	1D vertical - discrete	-		Wei et al. (2020)
Ti6Al4V	In718	1D vertical - step	Ti_2Ni	Cracking when In718 > 20%, Lack of fusion	Scaramuccia et al. (2020)
Al-12Si	Al-3.5Cu-1.5Mg-1Si	Powder on plate - discrete	-		Wang et al. (2020)
AlSi10Mg	C18400 Cu	1D vertical - discrete	Al_2Cu	Cracking in Al, Porosity in Cu	Sing et al. (2015)
Pure Al	SS316L	Powder on plate - discrete	Fe_2Al_5	Flake at Al	Nguyen et al. (2019)
W	Cu	Powder on plate - discrete	-	Cracking	Tan et al. (2019)

3 Multi-material interfacial characteristics

The manufacturing community is interested by MMLPBF because it provides the capability of joining dissimilar metals while leveraging the advantages of LPBF AM. This technology can lead to profound impacts by changing the current design philosophy, i.e., the transition from the conventional geometrical-based design based on single material properties to the functionally-graded design concepts that require location dependent properties (Li et al., 2020). As discussed in the previous section, there are many integration related technical challenges for realizing MMLPBF including the pre-processing software, the multi-material feedstock delivery, the machine control capabilities, and the post-processing heat treatments. From the materials science perspective, constructing a mechanically sound component requires a strong interface between the dissimilar metals. The interfacial alloying compositions often violate the traditional alloying design guidelines as many interfaces are essentially made by mixing large quantities of elements with different electronic layers, atomic sizes, and crystal structures. The properties of these alloying mixtures are often unknown. Additionally, the different thermophysical properties of the dissimilar metals, such as the melting point, the coefficient of thermal expansion (CTE), and the solubility, can lead to unique microstructures and problems, such as cracking, which are detrimental to the part integrity.

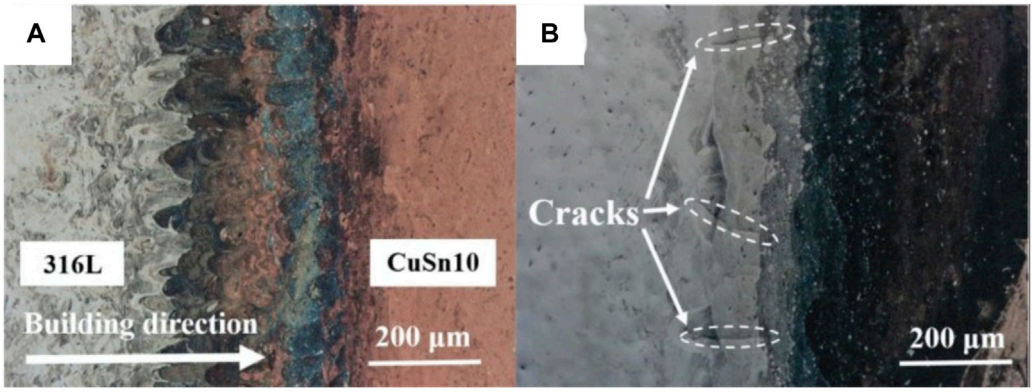

FIGURE 2
Optical image of the 316L/CuSn10 interface highlighting **(A)** the melt pool and material transition and **(B)** interfacial cracking at the 316L side. From Chen (K) et al. (2020).

Intermetallic phases may also form at specific composition ratios within the interface region. From the process control perspective, the interface introduces additional complexities to the selection of laser parameters given the ever-changing local composition. Process related defects, such as lack-of-fusion and loss of alloying elements often occur due to suboptimal laser energy inputs. All these problems need to be resolved before MMLPBF can be utilized as a production tool like the single-material LPBF. In this section, we will discuss the features and problems at the dissimilar metal interfaces as summarized in Table 2 followed by the technical difficulties and possible solutions.

3.1 Interfacial cracking

Cracking is a persistent problem during the material development for the single material LPBF due to the extreme cooling rate that is inherent to the process. The causes of the cracking problem can be the different solidus and liquidus temperatures at solidification (e.g., liquidus cracking and solidus cracking) or the solid-state phase transformation, precipitation, and property change (e.g., ductility-dip cracking and strain-age cracking). On the other hand, cracking mechanisms like liquid metal embrittlement (LME), cracking at the intermetallic phases and cracking at the fusion zone due to the mismatched CTEs are unique to MMLPBF.

The recent review paper of Wei and Li (2021) nicely described the LME defect in MMLPBF using the Galvele's atomic surface mobility model (Galvele, 1987). The LME induced cracking is susceptible when the interfacing solid and liquid phases have low miscibility. The larger difference between the melting points of the dissimilar alloys also accelerates the LME cracking. In MMLPBF, the LME cracking is a frequently reported problem for the Cu-Fe systems, which are desired for the fabrication of heat exchangers given the high thermal conductivity of copper alloys and the good high temperature strength and corrosion resistance of steels. At the interface of liquid copper and solid iron, the vacancies exchange and accumulate as the copper atoms diffuse into the iron grains, to form macroscopic defects at the interface that could result in crack initiation under the influence of residual stress. Several studies of MMLPBF Cu-Fe systems (Al-Jamal et al., 2008; Anstaett et al., 2017; Chen K. et al., 2020) reported the formation of microcracks at the interface as shown in Figure 2. As indicated by some of these studies, the formation of cracks could be complicated and is often attributed to multiple mechanisms which are difficult to deconvolute from each other. Both Chen K. et al. (2020) and Anstaett et al. (2017) suggest that the rapid solidification of the copper alloy could initiate cracks in the solidified steel region due to the different CTEs.

Similarly, some brittle intermetallic phases may form at certain composition ratios. The segregated intermetallic phases are susceptible crack initiation sites and preferred crack propagation paths under the cooling induced residual stress. Their CTEs and elastic moduli may be significantly different from those of the primary phase resulting in additional stress. In the graded material from Ti-6Al-4V to Invar 36 built by directed energy deposition (DED), Bobbio et al. (2017) experimentally identified the formation of the intermetallic phases (FeTi, Fe_2Ti, Ni_3Ti, and $NiTi_2$) in the transition region. The stress between the segregated phases, FeTi and Fe_2Ti, developed during rapid cooling exceeded 4 GPa and eventually led to cracking in the as-built specimens. Similar defects could occur in MMLPBF systems.

3.2 Process related defects and microstructural features

Process related defects like keyhole pores and lack-of-fusion in single material LPBF have been extensively studied (Martin et al., 2019; Mostafaei et al., 2022). Their formations are mainly driven by the suboptimal laser energy input. In MMLPBF, the additional materials bring another level of challenges to the optimization of the laser parameters because the optimal laser parameters will depend on the local compositions. That said, the ever-changing local thermophysical properties near the interface, which are often unknown, need to be considered in the optimization.

The high hardness and wear resistance of ceramics is of interest for high temperature and abrasive environment applications, e.g., TiB_2/Ti-6Al-4V. Chen et al. (2019) coupled finite element

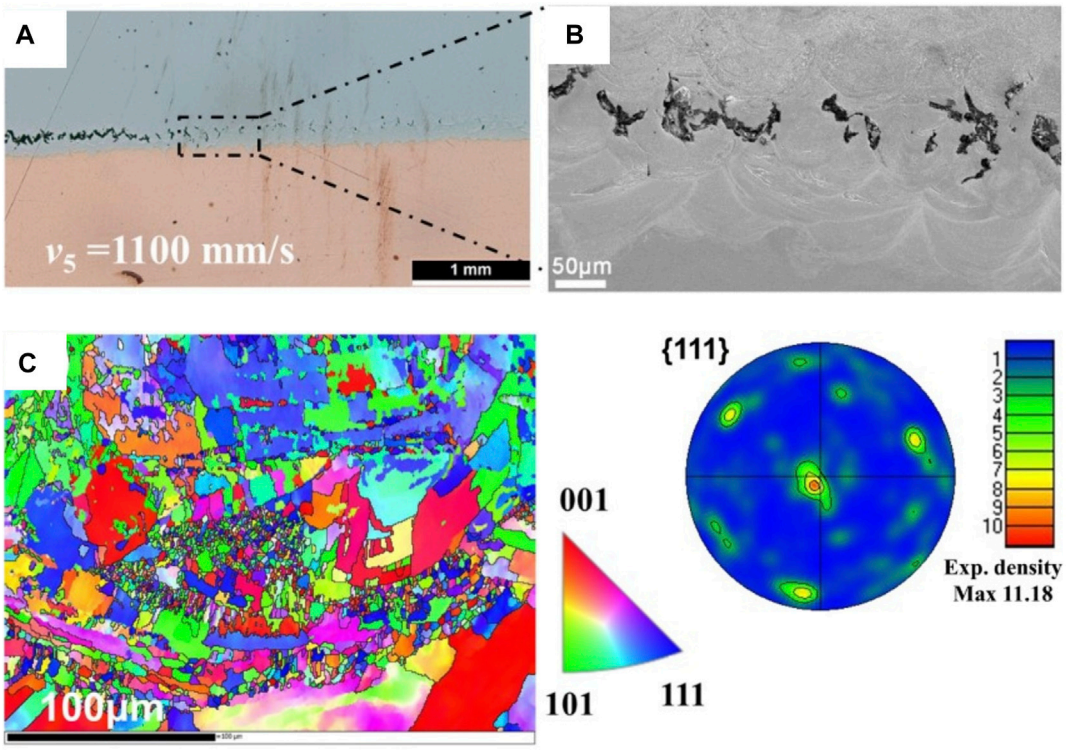

FIGURE 3
The maraging steel-copper interface of the hybrid SLM-produced specimen observed by optical microscope (OM), scanning electron microscope (SEM), and electron backscatter diffraction (EBSD): **(A)** lack-of-fusion defects in the maraging steel region, **(B)** the magnified view of the lack-of-fusion defects in **(A)**, and **(C)** the color inverse pole figure (IPF) and pole figure (PF) showing the grain orientation. From Tan et al. (2018).

simulations with experiments in MMLPBF to show that the liquid lifetime, the maximum temperature, and the configurations of the melt pool are critical for the interfacial quality especially when the two materials have very different melting points. Adjusting laser parameters could either benefit the wettability at the interface or lead to the formation of defects due to the capillary instability at the extreme energy levels.

Interfacing materials with different thermal conductivities can also result in the formation of defects and unique microstructures. At the interface of maraging steel and copper, Tan et al. (2018) reported that the onset of lack-of-fusion (Figure 3) occurred at higher laser energy densities for the maraging steel due to the rapid heat dissipation through the more conductive copper base. The high thermal conductivity also caused grain refinement and resulted in stronger <111> texture along the largest thermal gradient as shown in Figure 3.

The process parameters, the boundary orientation, and the thermophysical properties of the materials affect the width of the interface. To attain high compositional precision in components, it is important to understand the width of the interface. Bai et al. (2020) evaluated the interfacial characteristics of the dual interfaces between 316L steel and C52400 copper alloy. As shown in Figure 4, the 316L/C52400 interface (~200 μm) is significantly wider than the C52400/316L interface. One reason is that the laser parameters of printing 316L are different from those for printing C52400. More importantly, the different thermal conductivities of the substrates magnified the effects from the laser parameters, which in turn changed the remelting behaviors at the interface. Some isolated alloy islands, as highlighted by the blue arrows in Figure 4, were found at locations away from the interface. High undercooling and non-uniform metal liquid flow could be responsible for the formation of these islands.

In the compositionally graded area, the variation of the liquidus/solidus temperatures are mostly non-linear and often raise challenges to the parameter selection. As shown in Figure 5, Bobbio et al. (2017) reported that materials overflowed at the transition region from Ti-6Al-4V to Invar 36 where the liquidus/solidus temperatures dropped at 12—18 vol% of Invar. Excessive remelting occurred even though the process parameters were constant. Note that this example of overflow was observed in a DED process; however, the MMLPBF is also susceptible to overflow at the transition. The outcomes of the varying liquidus/solidus temperatures may be different in the two processes as the MMLPBF parts are supported by the surrounding powder bed. It is expected to see changes in porosity population and surface texture.

As discussed in the previous section, to achieve three-dimensional material gradient/interface it is inevitable to incorporate non-contact powder deposition methods into the spreading process. The multi-material spreader of Wei et al. (2018) utilized a vacuum sucker and a ultrasonic dispenser array to deposit the secondary powder. A higher defect population was found in ultrasonic deposition area. They suggested that the low powder compression and the uneven powder layer were responsible for the defect formation.

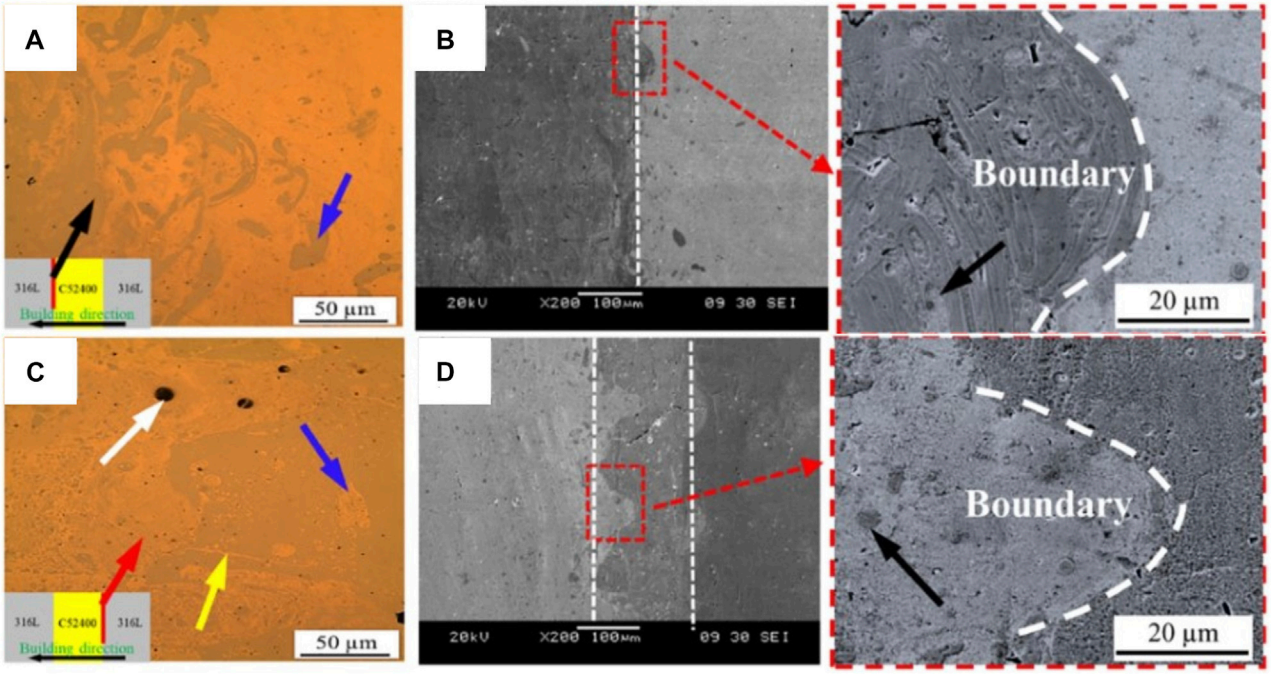

FIGURE 4
The optical and the SEM images showing the C52400/316L interface **(A, B)** and the 316L/C52400 interface **(C, D)**. Note that the blue arrow indicates the alloy islands away from the interface, the white arrow indicates a potential keyhole pore, the yellow arrow indicates a crack, and the black and red arrows indicate the prescribed interfaces. From Bai et al. (2020).

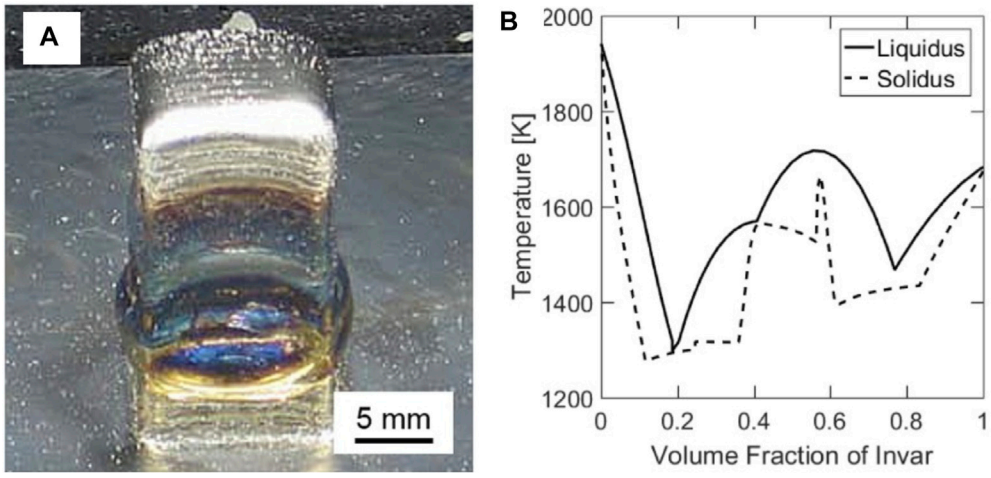

FIGURE 5
(A) Images of the functionally graded part from Ti-6Al-4V to Invar 36 showing the overflow problem due to the sudden dip of the liquidus/solidus temperatures at 18 vol% Invar as shown in **(B)**. From Bobbio et al. (2017).

3.3 Existing and potential solutions to mitigate interfacial defects

Certain material interfaces are difficult to fabricate due to the formation of brittle intermetallic compounds and distinct solidification and shrinkage behaviors which can lead to fracture and delamination. An approach to join these dissimilar materials is to introduce a third material which can form defect-free interfaces with the two primary alloys. Tey et al. (2020) successfully demonstrated a steep material transition from 316L stainless steel to Ti-6Al-4V by adding an interlayer of copper alloy. Another approach is to turn a discrete material interface into a gradient

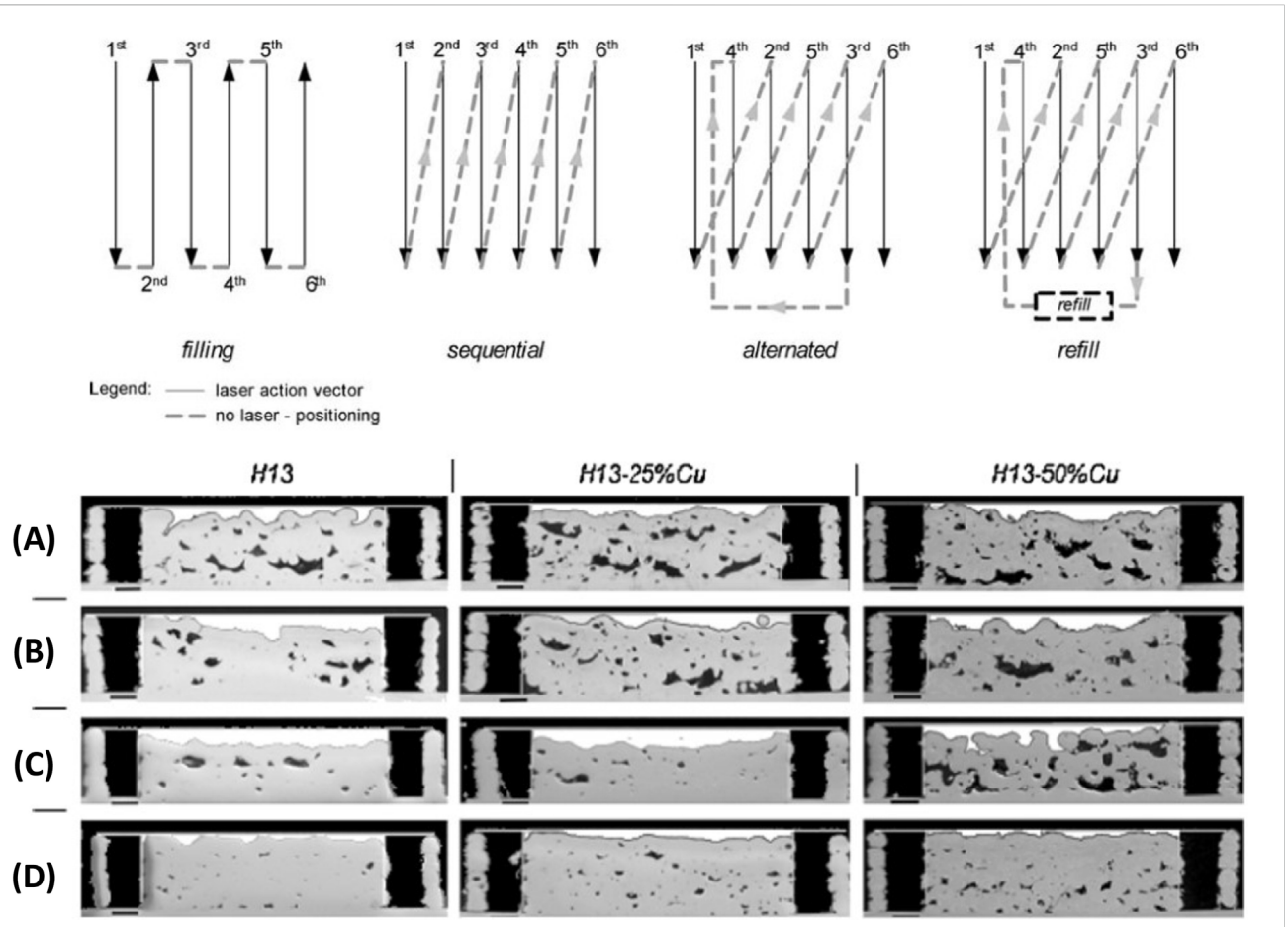

FIGURE 6
The schematics of the four laser scanning strategies applied in the fabrications of H13/Cu interfaces and the cross-sections of the resulted specimens at three different composition ratios. Note that **(A, B, C)** and **(D)** correspond to the filling, sequential, alternated, and refill scanning strategies. From Beal et al. (2006).

material region to minimize the mismatches of the thermophysical properties of the different composition ratios. This approach has been extensively tested in DED process owing to its capability of pre-mixing powder before powder delivery.

Several studies have discussed the possibility of using simulation approach to improve the interfacial quality. Bobbio et al. (2017) performed thermodynamic calculation using CALPHAD to identify the possible phases in a Ti-6Al-4V/Invar interface. The simulation results can help with the selection of composition ratios at the interface to avoid the formation of detrimental phases. Simulation approaches can also benefit the optimization of laser parameters. Chen et al. (2019) used finite element thermal simulation to identify the process parameters that can result in the optimal melt pool configurations and temperature distributions at the TiB_2/Ti-6Al-4V interface.

The recent effort of Scaramuccia et al. (2020) attempted to optimize the laser parameters for fabricating Ti-6Al-4V and Inconel 718 by mixing different composition ratios using an integrated powder mixer and creating a series of compositional steps over the entire gradient (called a step interface). This is an intermediate strategy of using multiple discrete interfaces to replace a single discrete interface. The study found the optimal energy densities for interfaces with <20 wt% Inconel 718; severe cracking occurred as the Inconel 718 content was above 20 wt% due to the formation of the Ti_2Ni intermetallic phase. This is a great example of finding the optimal laser parameters for the interface of dissimilar metals and identifying the composition ratios that may result in brittle intermetallic phases. The aforementioned CALPHAD approach can certainly benefit the selection of composition ratios in this situation.

To the authors' knowledge, no printer is capable of adjusting the laser parameters dynamically to deliver the optimal laser energy input according to the material compositions at the target. Knowing the optimized local composition and the corresponding laser parameters are the prerequisites of achieving dynamic laser parameter control in MMLPBF. As suggested by Binder et al. (2018), there are technical barriers that need to be overcome in the pre-processing step. The current data format of the print file only includes the surface representation of the object, and it is not able to assign different parameters to the regions with different compositions. It is important to utilize different print file formats, such as AMF (Additive Manufacturing File Format)

(ISO/ASTM 52915, 2020) during the pre-processing stage to enable location dependent parameters within the same part.

In addition to changing laser parameters, the scanning strategy can also be optimized for interfaces with different compositions. Beal et al. (2006) tested four scanning strategies for the H13 steel/Cu interface and showed that the interfaces with different composition ratios responded differently to the four scanning strategies as shown in Figure 6. Zhang et al. (2019) tested the remelting strategy on its ability to impact to the bonding strength of the CuSn/18Ni300 bimetallic interface.

3.4 Interface microstructure

Interface microstructure is an important research topic because it is critical to the performance of the multi-material AM components. Constantly varying local compositions may result in intermetallics and segregation; different thermophysical properties and interface orientations may affect the thermal history producing different grain sizes, morphology, and texture. All these present unique challenges of quantifying and comparing the microstructure in different material systems, which is compounded by the lack of universally agreed upon methods of evaluating the interface microstructure. Only a few comprehensive studies exist focusing on the interface microstructure and are discussed in this section. This presents a knowledge gap which is essential to the future development of multi-material additive manufacturing.

Chen K. et al. (2020) characterized the microstructure at the 316L/CuSn10 interface. The interface exhibits three different distinct regions, 1) 316L steel matrix zone, 2) interfacial region, and 3) CuSn10 matrix zone. The element distribution of the interfacial region is very uniform. All three regions display microscopic anisotropy, equiaxed grain morphology with grain size around 1 μm and various levels of recrystallization ratios. Wei et al. (2019) studied the 316L/Cu10Sn interface by characterizing the microstructure transitions along the step interfaces, i.e., multiple regions with constant ratios of the two alloys. They found that the microstructure started to separate to distinct phases as more Cu10Sn was added and segregation occurred at the interface of 25 vol% 316L/100 vol% Cu10Sn. The study detected phases like $Cu_{3.8}Ni$ and Cu_9NiSn_3 at the interface. Bai et al. (2020) evaluated the interfaces between 316L stainless steel and C5240 copper alloy and found that only face-center cubic structures formed at the interface, i.e., γ-Fe and ε-Cu phases. The microstructure exhibits strong texture and grain size variation depending on the local compositions. The grain size at the copper-steel interface is significantly smaller than the grain sizes in the single material areas. They hypothesized that the pre-solidified 316L offered the nucleation sites for the subsequent grain growth; this phenomenon is unique to multi-material printing.

Different from the Fe/Cu interfaces, the Ti/Cu interface resulted in more phases such as L_{21} ordered phase, amorphous phase, Ti_2Cu, and ε-Cu as reported by Tey et al. (2020). At the dissimilar interface of titanium alloys, Ti-5Al-2.5Sn/Ti-6Al-4V, Wei et al. (2020) showed that the epitaxial growth path of the prior-β grains crossed the interface and sustained for several millimeters. Martensitic transformation occurred because of the high cooling rate resulting the formation of the needle like α'. Microscopy indicated that the metastable α' martensitic microstructure within the Ti-5Al-2.5Sn region was fully recrystallized; by contrast, the recrystallization process did not occur in the Ti-6Al-4V portion due to the existence of the β stabilizer element V.

At the interface of aluminum alloys, Al-12Si and Al-Cu-Mg-Si, Wang et al. (2020) observed a more gradual transition of grain size and morphology. The columnar grains grew from 7.9 μm at the interface to 23.3 μm within the Al-Cu-Mg-Si region. Additionally, the relative amount of <001> fiber texture along the building direction at the interface is significantly higher compared with that in the single material region. Intermetallics are common at the dissimilar metal interface. At the interface of W-Cu, Tan et al. (2018) reported a trend of increasing tungsten grain size when moving away from the interface due to the high thermal conductivity of Cu. They also revealed the random orientation of the columnar grains within the tungsten region which was attributed to the laser scanning strategy with 67° rotation.

4 Mechanical properties

Mechanical property characterization is a fundamental part of the quantification and qualification of new material systems. In additive manufacturing, mechanical testing has been an important method for comparing additively manufactured components with their wrought counterparts to show equivalence or improvements for existing materials (Shunmugavel et al., 2015; DebRoy et al., 2018). However, with the capability of manufacturing multi-materials via AM methods, applying traditional mechanical testing techniques to determine bulk and interfacial properties could be expanded to better evaluate the new AM approaches and material combinations. In this section, we review literature for mechanical testing of multi-material AM components, organized by the primary material used, while in the next section we suggest additional mechanical tests that may be useful for multi-material AM. Table 3 gives an overview of mechanical tests performed on different multi-material systems. An observation from this table is that the MMLPBF field primarily uses microhardness and uniaxial tension (UT) measurements, in various configurations, as shown in Figure 7, to assess multi-material interfaces and determine interfacial bonding, respectively.

4.1 Ferrous interfaces: non-stainless steel

An early feasibility study of multi-material LPBF fabricated three 1 mm tall regions starting with a pure iron region, followed by a 55 vol% Fe, 45 vol% Al-12Si region, and then a 100 vol% Al-12Si region (Demir and Previtali, 2017). The multi-material region had much higher microhardness (450–550 HV0.5) compared to the single materials, pure Fe (150–160 HV0.5) and Al-12Si (90–100 HV0.3), due to the formation of the FeAl intermetallic Other ferrous alloys have

TABLE 3 Summary of multi-material laser powder bed fusion studies that include mechanical test data. Materials are listed by their commonly known names. Uniaxial tension (UT) tests, if completed, are further described with the relationship of the loading direction and gradient as parallel (‖) or perpendicular (⊥).

Initial material	Added material(s)	Gradient direction & type	Mechanical tests	Citation
18Ni300	CuSn10	Vertical - discrete	microhardness, UT (⊥), lattice compression	Zhang et al. (2019)
316L	K220 Cu/Ti-6Al-4V	Vertical - interlayer sandwich	UT (⊥), nanoindentation	Tey et al. (2020)
316L	C253400 (Cu alloy)/ 316L	Vertical - sandwich	microhardness	Bai et al. (2020)
316L	IN718	Vertical - discrete	microhardness, UT (‖), 3PT bend, 3PT fatigue, nanoindentation	Duval-Chaneac et al. (2021)
316L	CuSn10	Vertical - discrete	UT (⊥), nanoindentation	Chen et al. (2020a)
316L	IN718	Vertical - alternating	microhardness	Yusuf et al. (2021)
316L	IN718/316L	Vertical - sandwich	microhardness, UT (⊥)	Mei et al. (2019)
316L	CuSn10	Vertical - discrete	microhardness, UT (‖ & ⊥), 3PT bend	Chen et al. (2019b)
316L	MS1	Vertical - discrete & continuous	microhardness	Nadimpalli et al. (2019)
316L	CuSn10	Vertical - discrete	microhardness, UT (‖ & ⊥), 3PT bend	Chen et al. (2020b)
316L & Hastelloy X	Hastelloy & 316L	Vertical - discrete	microhardness, 3PT bend, UT (⊥)	Rankouhi et al. (2022)
AlSi10Mg	C18400 (Cu alloy)	Vertical - discrete	microhardness, UT (‖)	Sing et al. (2015)
CoCr	18Ni300/CuSn10/316L	Vertical - discrete	microhardness, nanoindentation	Wang et al. (2021)
Fe	Al-12Si	Vertical - continuous	microhardness	Demir and Previtali (2017)
Fe-3Si & 34CrNiMo6	34CrNiMo6 & Fe-3Si	Vertical - discrete	microhardness, UT (⊥), high cycle fatigue	Andreiev et al. (2021)
IN718	Cu	Horizontal - discrete	microhardness	Marques et al. (2022)
NiTi	Ti-6Al-4V	Vertical - cellular structure	microhardness, shear, nanoindentation	Bartolomeu et al. (2020)
Ti	Ti-6Al-4V	Vertical - discrete, sandwich, multiple	microhardness, UT (‖ & ⊥)	Borisov et al. (2021)
Ti-5Al-2.5Sn	Ti-6Al-4V	Vertical - discrete	microhardness, UT (⊥)	Wei et al. (2020)
Ti-6Al-4V	IN718	Vertical - continuous	microhardness	Scaramuccia et al. (2020)
Ti-6Al-4V	TiB2	Vertical - continuous	microhardness, lattice compression	Zhang et al. (2020)
W	316L/CuSn10	Vertical - interlayer sandwich	microhardness	Wei et al. (2022)

also been studied, an iron-silicon alloy (Fe–3Si) and a quenched and tempered steel (34CrNiMo6) build had a 120—150 μm thick interface that exhibited good metallurgical bonding independent of what alloy was the base material or built first (Andreiev et al., 2021). The interface, characterized via microhardness, linearly increased and decreased from the Fe–3Si with an average hardness of 225 HV0.3 to 34CrNiMo with an average hardness of 495 HV0.3, depending on the build order. The UT specimens always broke in the Fe-3Si part in both build arrangements and exhibited properties similar to the individual Fe-3Si samples. High-cycle fatigue of the bimetallic samples after being annealed at 850 °C, quenched in oil, and then annealed/tempered at 550 °C had fatigue properties similar to the Fe-3Si samples. There are too few studies on ferrous interfaces to make a broad conclusion about the mechanical response of these materials in MMLPBF.

4.2 Stainless steel interfaces

Stainless steel 316L is one of the most widely studied materials in multi-material LPBF processes, as shown in Table 2, Table 3. The face centered cubic (FCC) 316L alloy exhibits good ultimate tensile strength (630 MPa), Vickers microhardness (220 HV), and ductility (64% elongation to failure) as an as-built LPBF material (Sun et al., 2016; Wilson-Heid et al., 2019). In addition to the mechanical properties, 316L is also of interest in multi-material systems because of the materials corrosion resistance, which makes it a good pair for materials that do not exhibit the same properties. The existing process parameter knowledge base for manufacturing dense 316L samples is relatively extensive in the single-material LPBF community. This allows for studies to focus on the unique aspects of MMLPBF, such as hardness changes across an interface or build material order effects, after

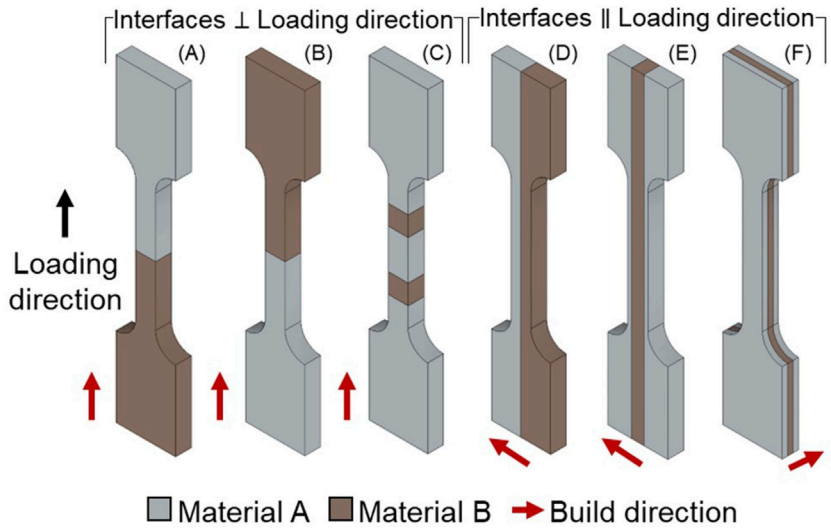

FIGURE 7
A compilation of LPBF bi-material uniaxial tension specimens that have been used in the literature. **(A)** and **(B)** are single perpendicular interface samples and are often paired in studies to determine build order effects. **(C)** simultaneously evaluates multiple perpendicular interfaces, **(D)** is often used to compare properties to **(A)** or **(B)**, and **(D–F)** evaluate interfaces parallel to the loading direction in multiple configurations. **(C–F)** are adapted from Borisov et al. (2021).

adding materials to 316L and not parameter development of the alloy.

The interface of maraging steel MS1 and 316L was characterized with Vickers microhardness across both discrete and gradient transitions, 12.5 wt% MS1 addition into 316L every five layers of until 100 wt% MS1. The microhardness in the gradient sample had a less abrupt change in hardness within 100 μm on either side of the interface compared to the discrete interface, whose microhardness increased in a similar trend to the wt% added of MS1 (Nadimpalli et al., 2019).

Inconel 718, also an FCC alloy, added to 316L has been studied because of the benefits of added high temperature mechanical properties, observed in both wrought and LPBF conditions (Sanchez et al., 2021). Using microhardness to evaluate the 100 μm fusion zone between the two materials, Yusuf et al. (2021) found an average hardness of 265 HV0.1 compared to 304 HV0.1 and 223 HV0.1 at the individual IN718 and 316L regions, respectively. The intermediate hardness in the fusion zone was attributed a lack of low-angle grain boundaries compared to those observed in the IN718 region, although both regions possessed a large fraction of high-angle grain boundaries. Other studies have also measured microhardness across the 316L-IN718 interface and found an intermediate hardness of the two primary constituents in the fusion zone (Mei et al., 2019; Duval-Chaneac et al., 2021). Duval-Chaneac et al. (2021) evaluated the fatigue properties of the 316L-IN718 multi-material system using notched three-point bend samples, where the interface boundary for the fatigue samples was perpendicular to the loading direction and found that in a sample with a single interface there was elemental partitioning that weakened the interdendritic areas and lead to decohesion and fast crack propagation. However, in a 4-layer fatigue bending sample, the multiple interfaces provided crack shielding that decreased crack growth rate in the additional interface leading to improved fatigue performance relative to the bi-layer specimen, which shows the importance of testing many configurations of the multi-material systems.

Rankouhi et al. (2022) tested Hastelloy X (HX), another FCC nickel superalloy, bonded to 316L through a combination of tensile and 3-point bend tests and determined a strong 240 μm fusion zone was formed. In the UT tests, failure occurred away from the interface in the 316L region and had similar strength to 316L alone, but lower average failure strain (43.8%) compared to HX (62.1%) and 316L (62.7%) as shown in Figure 8. In both the UT and 3-point bend tests no evidence of cracking or voids were found at the interfaces.

4.3 Stainless steel and copper alloy interfaces

Copper and its alloys are of interest in the multi-material AM community because of potential applications to add highly conductive regions of components that would boost performance capabilities. Pairing copper with another material that possesses complimentary and improved mechanical properties such as 316L is an appealing application for multi-material LPBF.

In two studies by Chen et al., the 316L and CuSn10 tin-bronze system was explored (Chen J. et al., 2019; Chen et al., 2020 J.). They reported a 243 μm wide fusion zone without defects, a width that was in the middle of all recorded values after a broad sweep of process parameters, resulted in the best UT properties with the joint ultimate strength of 460 MPa and elongation to failure of 5%; the tests were conducted with the loading direction perpendicular to the interface (Chen J. et al., 2019; Chen et al., 2020 J.). Uniaxial tension tests parallel to the interface were lower performing than the two alloys alone. Nanoindentation characterization of the interface revealed a higher nano-hardness in the interface (2.97 GPa)

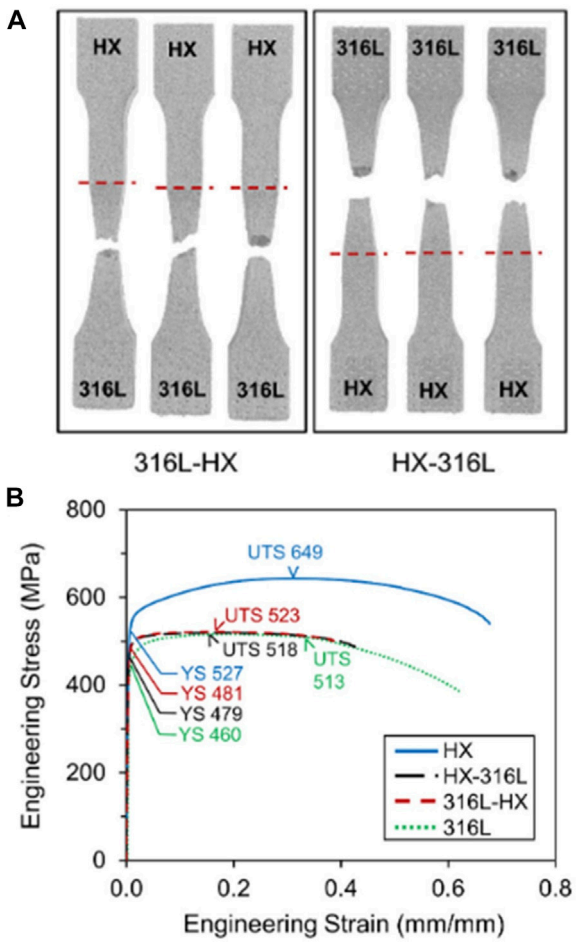

FIGURE 8
Tensile test results of 316 L, Hastelloy X, and multi-material samples. **(A)** failed samples, **(B)** representative stress-strain curves. The red dashed lines indicate the interface. These tests show how the multi-material properties were independent of the material build order during fabrication, where the 316L-HX were built with 316L on the build plate and *vice versa* for the HX.

compared to either of the constituents, which was attributed to fine grains in the interfacial region. However, Vickers microhardness does not show an increase at the fusion zone, but rather was an intermediate value between the two alloys. This is in contrast to another study of the same material interface where both microhardness and nano-hardness were found to be higher in the interface of 316L and CuSn10, where they attributed this finding to the formation a new intermetallic phase (Wang et al., 2021). Finally, 3-point bend tests revealed dendritic cracks near the boundary that resulted in lower maximum flexural strength in the multi-material samples. Evaluating the same system other authors found the flexural strength of 316L/CuSn10 was between 316L and CuSn10, regardless of which material was used as the base material (Chen K. et al., 2020).

The 316L/CuSn10 interface was the focus of another study that used 316L material as an intermediate step in the fabrication of tungsten W) to CuSn10 multi-material parts and concluded that the addition of the 316L region was necessary as they were unable to successfully manufacture W/CuSn10 bimetallic components without delamination (Wei et al., 2022). In the evaluation of the interfaces in the three-alloy component the authors concluded that microhardness testing was inadequate for the W/316L interface because the large difference in microhardness led to slipping of the indenter tip, instead nano-hardness is necessary in fusion zones of materials with large differences in hardness.

Another copper alloy, C52400, was also used with 316L as the base material, but an additional interface was added on top of the copper alloy by sandwiching the copper with 316L, resulting in a 9 mm tall build where each section was 3 mm (Bai et al., 2020). Both interfaces, the 316L/C52400 and C52400/316L, were evaluated with Vickers microhardness measurements. In the first interface the hardness was intermediate between the two alloys gradually falling in the interface region. In the second interface, there was a high peak hardness that was attributed to lack of intermixing, which was also observed in another study with a different copper alloy where bands of 316L remained in the interface (Tey et al., 2020). Tey et al. (2020) used a copper alloy (HOVADUR® K220) as a thin interlayer to transition from 316L at the bottom to a Ti-6Al-4V region on the top of a build, as shown in Figure 9. In fractography of uniaxial tension tests the authors observed that in the copper alloy and Ti-6Al-4V interface region the α′-Ti phase that formed acted to arrest and deflect propagating cracks in the ductile copper alloy region improving the mechanical properties, where the sample with a higher concentration of α′-Ti phase had improved strength.

Further expanding the number of interfaces evaluated in a multi-material LPBF build, Wang et al. (2020) manufactured a four-alloy component consisting of base CoCrMo alloy, then 18Ni300, followed by CuSn10 and finally 316L. The familiar CuSn10/316L interface was the only interface where microcracks formed, and each interface had different fusion zone trends with respect to microhardness and nano-hardness. The 230 µm wide CoCrMo/18Ni300 interface had lower hardness that the constituents, the broader 345 µm wide 18Ni300/CuSn10 interface exhibited an intermediate hardness, and the narrowest 135 µm CuSn10/316L interface had a higher hardness than either alloy. The 18Ni300/CuSn10 interface was also examined in a different study that fabricated cylindrical uniaxial tension and lattice compression specimens (Zhang et al., 2019). The tensile properties of the multi-material samples were weaker than LPBF CuSn10 alone, 144.1 ± 41.59 MPa and 441.0 ± 7.048 MPa, respectively. However, the compression tests showed improved energy absorption properties in the bimetallic lattice structure relative to the LPBF CuSn10 fabricated in the same geometry. Testing bulk properties *versus* those in lattice geometries reveals that multi-material samples may be best used in a variety of different applications and should be evaluated across a wide array of test geometries to determine the proper application space.

4.4 Copper alloys with other materials

Other alloys have also been explored for bonding with copper alloys with specific applications in mind such as in heat exchangers and electrical connectors (Sing et al., 2015; Marques et al., 2022).

In the study of components with a discrete gradient between UNS C18400 copper alloy and AlSi10Mg the bimetallic UT

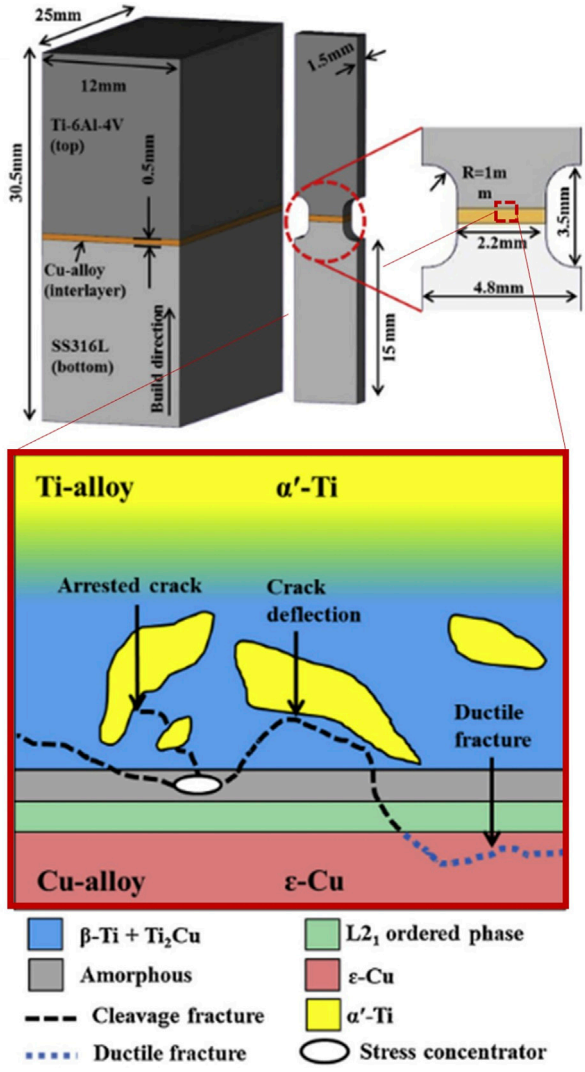

FIGURE 9
Using an interlayer between two materials can result in better material bonding. Build configuration of multi-material LPBF part and dimensions of the tensile sample with an illustration of fracture paths within the copper alloy and Ti-6Al-4V interface as determined with fractography. From Tey et al. (2020).

specimens, with the loading direction parallel to the interface, exhibited higher tensile strength (176 ± 31 MPa) than that of copper but lower than that of AlSi10Mg (Sing et al., 2015). The authors completed 3-point bend tests that showed a large difference in flexural strength depending on sample orientation, the flexural strength when the Cu alloy was on the bottom was 200 MPa and it was 500 MPa when the aluminum alloy was on the bottom. The variation in properties was hypothesized to be caused by the higher amount of porosity in the copper region that when in tension at the bottom of the samples led to earlier crack propagation and failure. This finding shows the potential to use materials that are more prone to porosity formation from LPBF processing in the component locations that are only designed to remain in compressive loading, while using more printable, dense alloys in tension loaded regions of the same component.

In an XY gradient structure of IN718 and pure Cu, that is the two materials are used on the same build layer instead of consecutive layers like a majority of the multi-material LPBF parts are, the Vickers microhardness measurements were unable to detect an independent hardness value of the thin 25 μm fusion zone and instead the parts had two distinct hardness values, 344 HV in the IN718 regions and 126 HV in the pure Cu regions (Marques et al., 2022). The XY multi-material components present an interesting opportunity to learn about interfacial bonding and as the field matures, further mechanical evaluations should be performed.

4.5 Titanium alloys

Titanium and its alloys, primarily Ti-6Al-4V, are used in a wide variety of applications ranging from use in aerospace, for their combination of the high strength and low density, to biomedical applications due to properties that promote biocompatibility (Peters et al., 2003; ASTM Standard F1108-21, 2021). In LPBF literature, Ti-6Al-4V has been extensively studied (Martin et al., 2019; Furton et al., 2021; Luo et al., 2022), which makes it an easier starting point for manufacturing multi-material components, similar to the usage of stainless steel 316L.

The effect of varying discrete interface configurations was evaluated in pure Ti and Ti-6Al-4V bimetallic components. Four variations of interfaces were fabricated, as shown in Figures 7C–F, the first three evaluated the interfaces parallel to the loading direction: a single interface down the length of the UT sample, a Ti/Ti-6Al-4V/Ti sandwich through the width of the flat UT sample, a Ti/Ti-6Al-4V/Ti sandwich through the thickness of the flat UT sample, and in the last variation the loading direction was perpendicular to two Ti-6Al-4V regions in the gauge section surrounded by Ti (Borisov et al., 2021). The authors found that the Ti-6Al-4V sandwich through the thickness of the flat UT sample resulted in the best mechanical behavior, exhibiting the highest UTS (839 ± 14 MPa) and elongation to failure (7% ± 3%) compared to the other bimetallic configurations, the strength was between the pure Ti (700 ± 12 MPa) and pure Ti-6Al-4V (998 ± 21 MPa) samples while the ductility was lower than both the Ti (16% ± 4%) and Ti-6Al-4V (10% ± 3%) only samples. The sample with worst UT properties were the bimetallic samples that had interfaces perpendicular to the loading direction, which highlighted the importance of understanding the loading orientations with respect to interfaces for multi-material parts built via LPBF.

In another study that primarily used UT tests to evaluate mechanical bonding, a Ti-6Al-4V and Ti-5Al-2.5Sn multi-material component was reported to have tensile strength and elongation to failure significantly lower than that of LPBF Ti-6Al-4V, but relatively close to that of LPBF Ti-5Al-2.5Sn (1,074 MPa and 7.7%, respectively) (Wei et al., 2020). The authors concluded that the softer Ti-5Al-2.5Sn determined the mechanical properties of the multi-material and not the 70 μm wide interface, built perpendicular to the loading direction, that was formed between the alloys.

In addition to using other Ti-based alloys, Ti-6Al-4V was graded to IN718 by Scaramuccia et al. (2020) in 10 wt% increments up to 40 wt% IN718 and then was transitioned to 100 wt% IN718. The gradual introduction of IN718 led to a measured microhardness in

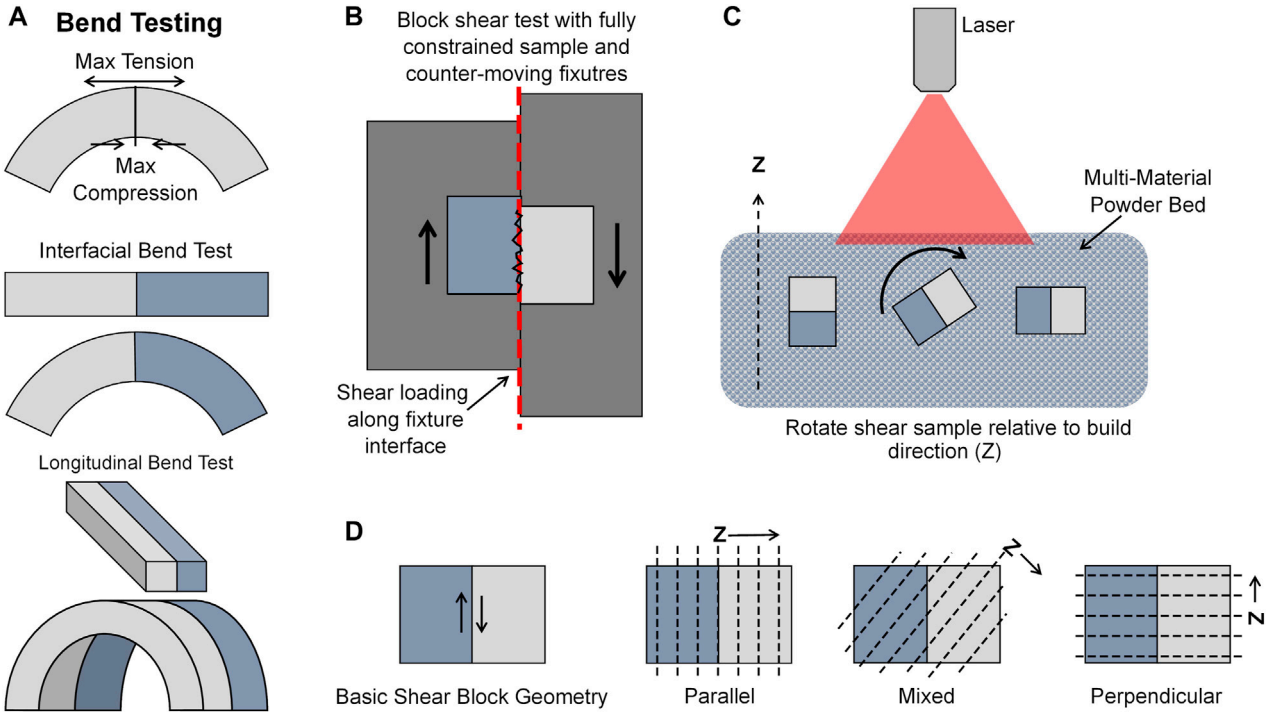

FIGURE 10
(A) Bend test schematics for MMLPBF testing including focused interface testing and across-length longitudinal testing, **(B)** diagram of a block shear test fixture for testing dissimilar material interfaces, **(C)** MMLPBF diagram showing shear test specimens being produced at varying angles within the build, **(D)** the basic multi-material shear block geometry and those with variable layer-to-layer and material-to-material interface angles. The dashed lines indicate layer boundaries in the build.

the 10 wt% IN718 region (381 ± 21 HV) to be lower than Ti-6Al-4V (402 ± 7 HV) due to the addition of beta phase stabilizers from the IN718 alloy. However, at 20–40 wt% the hardness increased dramatically to 477 ± 16 HV for 20 wt%, 684 ± 48 HV for 30 wt %, and 582 ± 27 HV for 40 wt% IN718 content, due to the formation of hard intermetallic phases that led to significant cracking in the 30 and 40 wt% samples, and then dropped back down to the expected lower hardness for 100 wt% IN718 (255 ± 13 HV). The formation of intermetallic phases can be detrimental to other mechanical properties and printability due to their brittle nature.

Shear bond tests were using to quantify the bonding strength of a NiTi and Ti-6Al-4V multi-material lattice structure with applications for biomedical hip implants (Bartolomeu et al., 2020). The shear bond test consisted of a custom-made sliding shear set-up where the shear load was applied to the transition region of the samples to determine the shear bonding strength of the fusion zone. The NiTi/Ti-6Al-4V samples had a shear strength of 33.2 ± 5.3 MPa, which was between the shear strength, of the two mono-materials evaluated with the same sample geometry, 25.5 ± 4.8 MPa and 47.1 ± 4.0 MPa for NiTi and Ti-6Al-4V, respectively. In a different porous cellular geometry, the Schoen Gyroid lattice structure, TiB_2 was added in increments of 1 wt%, up to 3 wt%, to a Ti-6Al-4V initial region (Zhang et al., 2020). Vickers microhardness was recorded in each region and the material exhibited an increase in hardness as a function of TiB_2 content going from 370.3 HV in the Ti-6Al-4V region to 428 HV with 3 wt% TiB_2. Compression tests of the gyroid structures revealed that compression stress-strain behavior of TiB/Ti-6Al-4V samples had a smaller elastoplastic stage and fracture strain than Ti-6Al-4V samples no matter the relative density of gyroid.

Titanium based MMLPBF studies have shown that build order and fusion zone orientation with respect to the loading direction, specifically in uniaxial tension tests, are important design criteria when evaluating mechanical performance of MMLPBF parts. The testing of AM specific geometries fabricated with multi-materials, presents both the challenges of correctly testing the geometry and interfaces simultaneously, although compression and shear tests have proven to be useful tests based on the expected applications of the structures.

5 Mechanical testing considerations in traditional dissimilar metal bonding

In addition to existing literature on mechanical testing of MMLPBF builds, it is worthwhile to consider contemporary literature on mechanical testing of non-AM dissimilar metal bonds. As many metal AM techniques, including LPBF, are based on conventional welding, mechanical tests for dissimilar welded joints are also likely to be appropriate for MMLPBF parts. Examples of electron beam and laser welding of dissimilar metals are abundant in literature. A recent review paper written by Fang et al. (2019) neatly summarizes current results in this field, focusing on studies which use a metallic interlayer to promote weld

strength. The review highlights mechanical test results from six laser welding and five electron-beam welding studies across a variety of metal-metal systems. Within these studies, several different mechanical characterization techniques are used including microhardness testing and mapping, as is seen in MMLPBF. Additionally, the majority of the reviewed papers use tensile tests as a final metric for bond strength and behavior. The review focuses on highly reactive metal systems, so nearly all of the test results show failure at the bond reaction interface due to high concentrations of embrittling intermetallic compounds. Outside of this collection, several other papers show tensile failure occurring in the softer of two materials for dissimilar metal welds when large concentrations of intermetallic compounds are not present (Rossini et al., 2015; Krishnaja et al., 2018; Xin et al., 2021). While these results support many of the similarities between dissimilar metal welding and LPBF, they fail to provide additional insight into testing which may better validate bond strengths required for MMLPBF to be used for true mesoscale design.

The review by Fang et al. (2019) also highlights the abundance of diffusion bonding literature and the differing nature of mechanical testing within these studies. Unlike fusion welding or LPBF, diffusion bonding is generally a low temperature process in which two materials in contact are brought to elevated, but sub-melting, temperatures and allowed to sit in contact until interatomic diffusion has proceeded far enough to create a bond between the materials. While interdiffusion can still result in the formation of intermetallic compounds, the reduced mixing and lack of a liquid phase for precipitation of these compounds generally reduces their concentration and distribution range (Mo et al., 2018). At a glance, diffusion bonding seems irrelevant to MMLPBF given the lack of melting and fusion, but it shares one key similarity: a potentially large surface area of bond region between dissimilar metals. While diffusion bonding typically focuses on large planar bonds, as that is easier to process, MMLPBF can result in similar bonded areas, albeit spread across more geometrically complicated regions.

While several of the diffusion bonding papers reviewed by Fang et al. (2019) use tensile tests to assess the bond, a large number use various types of shear test apparatus. Though not strictly mentioned within these papers, shear tests were likely selected due to the geometry of bonds having the wrong orientation or length-scale for producing tensile specimens (i.e., plate-on-plate bond). While not strictly better than the uniaxial tension tests most frequently seen in LPBF and welding, there are several advantages of shear testing that merit consideration for MMLPBF studies. First, using the various shear test setups, one can force shear loading to occur exclusively in a certain region or band of material. For example, shear loading can be applied exclusively at the interface boundary or at varying distances from the interface in one material or another. This is in contrast to tensile tests where loading occurs across the full gauge, and differences in elasticity and strength may concentrate deformation and loading in certain regions. Second, shear loading is often more analogous to real world loading applications, and the failure modes seen within can give better inference into feasibility and use cases for a dissimilar metal bond than a tension test can. Finally, by testing directly on the boundary one can identify the effective mechanical characteristics of that region, an important necessity for modelling and design.

Considering the actual use case for MMLPBF, parts which fit geometric requirements for regular fusion welding would likely just use fusion welding due to its maturity. Instead, the most suitable application for MMLPBF is parts with large surface area of contact such as those generally processed via diffusion bonding or even conventional joinery (i.e., fasteners and bolts). Even more than just replacing conventional approaches, dissimilar metal LPBF merits the redesign of these parts as they would no longer be limited to flat, easy to bond interfaces and could leverage stronger or more optimized geometries based on mesoscale design. Given this high suitability to large bond area applications, the mechanical testing methods needed for design and optimization should reflect this. As reviewed prior, shear testing is the most suitable and abundant for these large area bonds, however tensile tests are still well suited to identifying stress risers and weak regions across the dissimilar interface.

In addition to shear and tensile tests, bending tests are another popular testing method for dissimilar metal welds (Avery, 1991; Taylor et al., 2006; Lee, 2019; Gene, 2022) and are seen more sparingly in MMLPBF literature (Chen J. et al., 2019; Chen J. et al., 2020; Duval-Chaneac et al., 2021; Rankhoui et al., 2022). Generally, the bend tests are run in one of two ways (Figure 10A). First, a longitudinal bend test with the bond interface along the length of the bending sample, and second, a focused test with the bond interface centered along the bar length where loading during bending is most intense. In longitudinal bend tests, the deformed or broken samples are often inspected for delamination or failure along the bond interface rather than the specific strength, making it useful for pointing out defects such as cracking, porosity or other stress risers that will cause the bend test to fail outside of the area of peak stress. Bend testing centered on the interface puts tensile and compressive loading across the interface which can be useful to identify failure modes and concentrates load at the interface more effectively than a tensile test. For many applications such as dissimilar pipe section joints (Taylor et al., 2006) bend tests can also be indicative of real world loading conditions.

Summarizing the literature from dissimilar metal welding and MMLPBF we recommend the following approaches to mechanical testing. First, microhardness testing and mapping is somewhat of a *de facto* approach, that while not mandatory, is extremely effective for rapidly assessing the softening and hardening that occurs in dissimilar metal bonds. This behavior is attributed to residual stresses, intermetallic compound formation, annealing, and potential cracking or porosity, with delineation between these requiring complementary microstructural characterization such as that presented in Section 3. Tensile tests across the bond are useful for rapidly assessing failure prone regions but are limited to only providing meaningful information on this specific region rather than across the entire bond. Bend tests can help isolate loading to different regions across the bond or spread it evenly across a bond to test lamination and overall bond soundness. The complex loading across the sample, however, can provide less useable information than tensile or shear tests, with a key exception being final applications where the dissimilar bond will face bending conditions. Finally, shear testing (Figure 10B) is an underutilized technique that can isolate loading to specific regions across a dissimilar metal bond, providing effective

mechanical characteristics about the bond relevant to use in modelling and design of complex, large surface area dissimilar material bonds that are facilitated by MMLPBF.

Figure 10C shows a series of samples that could be procedurally built and tested in shear to provide meaningful bond characteristics for mesoscale design of multi-metal parts. Here we recommend a "lug" or "block" shear configuration (fully-constrained) due the strong ability to isolate loading across specific regions and ease of production as compared to some other samples such as those for lap shear tests. In this test approach the position of the interface relevant to the shear loading can be adjusted either by changing sample dimensions or with flexible fixturing approaches using spacers or interchangeable grips. This allows for direct shear loading and testing at select sites, for example, at the bond interface, in a heat affected zone, or at complex angles to the bond. By producing three or more samples at different rotations relative to the build direction of an LPBF machine one can identify variability of bond behavior and strength at different orientations, which is necessary for true meso-scale design capabilities in MMLPBF. This is expected to be particularly important given the single dimensionality of laser or beam application in LPBF, that is the melt pool is always applied top down and the bonding and mixing behavior between materials stacked on top of one another and those side by side will often be different due to different melting and solidification behavior, including the stress states, reactions, and bonding that occur due to this.

In summary, we believe shear tests may be the most appropriate and least utilized for characterizing these dissimilar bonds as well as producing data relevant to modelling needs. This is likely in part due to the lack of standardized equipment and methods for these types of tests, with many load-frame rigs being custom made and designed. In addition, many standards are designed for testing conventional fasteners and adhesives rather than the metallurgical bonds in welding and LPBF (ASTM Standard D4501-01, 2014). Finally, we note that the recommendation and format proposed here is not all encompassing and there are many other forms of shear tests which can be performed and may be more relevant to a specific application, limitations in machine capacity or dimensionality of multi-material feed capabilities.

6 Conclusion

Dissimilar metal bonding provides the opportunity for new design and optimization in a variety of applications such as wear and corrosion resistance, light weighting, and dynamic mechanical performance. The site-by-site buildup of material in additive manufacturing, when paired with multi-material capabilities, provides the opportunity for meso-scale design which can realize such opportunities. Inarguably the most studied metal AM process, laser powder bed fusion, multi-material metal processing is an active, but somewhat niche topic. Here we identified the current capabilities and limitations of MMLPBF, noting the lack of comprehensive and consistent mechanical testing in the area, the results of which are necessary for true meso-scale design use cases. The conclusions from this review of the state-of-the-art in MMLPBF are as follows.

- Current capabilities readily provide 1-dimensional feed of different metals for MMLPBF but lack the robustness and flexibility to accurately provide 3-dimensional feed needed for true meso-scale design. While improvements are occurring in this area, attention must be paid to 1) the quality of the powder bed, 2) the compositional dependent laser parameters, 3) the formation of intermetallic phases, and 4) the mismatching thermo-physical properties of the dissimilar metals to avoid common defects unrelated to multiple material bonding.
- The interfacial microstructures can have unique features, such as highly anisotropic textures and heterogeneous mixing due to the different thermal histories and material properties. They clearly influence the appearance of the interfaces. However, there are limited comprehensive studies that connect the microstructural features with the joint quality and performance.
- Several potential ways may improve the interfacial quality, including 1) optimizing laser parameters and scan strategies, 2) optimizing the interfacial geometry, 3) reducing the mismatches of the thermo-physical properties by using modeling approach. Some approaches, e.g., compositional dependent laser parameters, require additional infrastructural development during the pre-processing and the processing stage.
- The number of studies that include both microstructural properties and mechanical tests data is low. As such, it is difficult to recognize trends in mechanical properties as influenced by part microstructure. Further work is needed to correlate microstructural properties and mechanical strength in MMLPBF built parts.
- The number of MMLPBF studies which include mechanical tests outside of microhardness is low, and those that do are almost entirely limited to tensile tests. For several reasons these tensile tests can be insufficient to truly identify mechanical properties of MMLPBF parts and necessitates further consideration.
- Testing interfaces in configurations close to the envisioned applications is important because of the unique relationships between interface area, bonding depth, and loading direction. In considering testing methods, researchers should carefully examine the loading orientations with respect to the gradient direction ensure the interface is test over a wide range of loading conditions.
- Looking outward to other dissimilar metal bonding techniques we highlight shear testing as a robust technique, better suited to identifying regional interface characteristics relevant to modelling and design.
- While much simulation work as been done to understand LPBF in general, the application of these approaches to MMLPBF is still limited. Suitable simulations studies may offer significant insight into needed process parameter variation or microstructural evolution.

In conclusion, while multi-material LPBF is a rapidly growing field, it is apparent that more robust mechanical characterization of the interface between two materials is needed before full scale parts can be readily designed and produced. The mechanical tests should be tailored to give information about the interface under relevant loading conditions to the end use. Finally, more care should be given to mapping process parameters to final part quality to determine

more complicated relationships between part quality and laser power, laser speed, or other build parameters.

Author contributions

All authors listed have made a substantial, direct, and intellectual contribution to the work, including conceptualization, visualization, writing—original draft, writing—review & editing, and approved it for publication.

Funding

EE and ZW were supported by the LLNL-LDRD Program under Project No. 22-ERD-018.

Acknowledgments

This work was performed under the auspices of the U.S. Department of Energy by Lawrence Livermore National Laboratory under Contract DE-AC52-07NA27344. IM# LLNL-JRNL-841687.

Conflict of interest

Author ESE has patent #US20210260822A1 pending to Lawrence Livermore National Security LLC.

The remaining authors declare that the research was conducted in the absence of any commercial or financial relationships that could be construed as a potential conflict of interest.

Publisher's note

All claims expressed in this article are solely those of the authors and do not necessarily represent those of their affiliated organizations, or those of the publisher, the editors and the reviewers. Any product that may be evaluated in this article, or claim that may be made by its manufacturer, is not guaranteed or endorsed by the publisher.

References

Aerosint - Multi-Material 3D Printing (2022). Aerosint. Available at: https://aerosint.com/(Accessed October 4, 2022).

Al-Jamal, O. M., Hinduja, S., and Li, L. (2008). Characteristics of the bond in Cu–H13 tool steel parts fabricated using SLM. *CIRP Ann.* 57, 239–242. doi:10.1016/j.cirp.2008.03.010

Andreiev, A., Hoyer, K.-P., Dula, D., Hengsbach, F., Grydin, O., Frolov, Y., et al. (2021). Laser beam melting of functionally graded materials with application-adapted tailoring of magnetic and mechanical performance. *Mater. Sci. Eng. A* 822, 141662. doi:10.1016/j.msea.2021.141662

Anstaett, C., Schafnitzel, M., Seidel, C., and Reinhart, G. (October 2017). "Laser-based powder bed fusion of 3D-multi-material-parts of copper-chrome-zirconia and tool steel," in Proceedings of the Euro PM2017 proceedings: AM - beam based technologies, Milan, Italy .

Anstaett, C., and Seidel, C. (2016). Multi-material processing. *Laser Tech. J.* 13, 28–31. doi:10.1002/latj.201600027

ASTM Standard D4501-01 (2014). Standard test method for shear strength of adhesive bonds between rigid substrates by the block-shear method. (Accessed October 10, 2022). doi:10.1520/D4501-01R14

ASTM Standard F1108-21 (2021). Standard specification for Titanium-6Aluminum-4Vanadium alloy castings for surgical implants (UNS R56406). (Accessed October 12, 2022). doi:10.1520/F1108-21

Avery, R. E. (1991). Pay attention to dissimilar-metal welds: Guidelines for welding dissimilar metals. *NiDI Repr. Ser.* 14, 1–5.

Bai, Y., Zhang, J., Zhao, C., Li, C., and Wang, H. (2020). Dual interfacial characterization and property in multi-material selective laser melting of 316L stainless steel and C52400 copper alloy. *Mater. Charact.* 167, 110489. doi:10.1016/j.matchar.2020.110489

Bartolomeu, F., Costa, M. M., Alves, N., Miranda, G., and Silva, F. S. (2020). Additive manufacturing of NiTi-Ti6Al4V multi-material cellular structures targeting orthopedic implants. *Opt. Lasers Eng.* 134, 106208. doi:10.1016/j.optlaseng.2020.106208

Beal, V. E., Erasenthiran, P., Hopkinson, N., Dickens, P., and Ahrens, C. H. (2006). The effect of scanning strategy on laser fusion of functionally graded H13/Cu materials. *Int. J. Adv. Manuf. Technol.* 30, 844–852. doi:10.1007/s00170-005-0130-x

Bhaduri, D., Penchev, P., Essa, K., Dimov, S., Carter, L. N., Pruncu, C. I., et al. (2019). Evaluation of surface/interface quality, microstructure and mechanical properties of hybrid additive-subtractive aluminium parts. *CIRP Ann.* 68, 237–240. doi:10.1016/j.cirp.2019.04.116

Binder, M., Anstaett, C., Horn, M., Herzer, F., Schlick, G., Seidel, C., et al. (2018). "Potentials and challenges of multi-material processing by laser-based powder bed fusion," in *2018 international solid freeform fabrication symposium*. doi:10.26153/tsw/17025

Bobbio, L. D., Bocklund, B., Otis, R., Borgonia, J. P., Dillon, R. P., Shapiro, A. A., et al. (2018). Characterization of a functionally graded material of Ti-6Al-4V to 304L stainless steel with an intermediate V section. *J. Alloys Compd.* 742, 1031–1036. doi:10.1016/j.jallcom.2018.01.156

Bobbio, L. D., Otis, R. A., Borgonia, J. P., Dillon, R. P., Shapiro, A. A., Liu, Z.-K., et al. (2017). Additive manufacturing of a functionally graded material from Ti-6Al-4V to Invar: Experimental characterization and thermodynamic calculations. *Acta Mater.* 127, 133–142. doi:10.1016/j.actamat.2016.12.070

Borisov, E., Polozov, I., Starikov, K., Popovich, A., and Sufiiarov, V. (2021). Structure and properties of Ti/Ti64 graded material manufactured by laser powder bed fusion. *Materials* 14, 6140. doi:10.3390/ma14206140

Chen, C., Gu, D., Dai, D., Du, L., Wang, R., Ma, C., et al. (2019a). Laser additive manufacturing of layered TiB2/Ti6Al4V multi-material parts: Understanding thermal behavior evolution. *Opt. Laser Technol.* 119, 105666. doi:10.1016/j.optlastec.2019.105666

Chen, J., Yang, Y., Song, C., Wang, D., Wu, S., and Zhang, M. (2020a). Influence mechanism of process parameters on the interfacial characterization of selective laser melting 316L/CuSn10. *Mater. Sci. Eng. A* 792, 139316. doi:10.1016/j.msea.2020.139316

Chen, J., Yang, Y., Song, C., Zhang, M., Wu, S., and Wang, D. (2019b). Interfacial microstructure and mechanical properties of 316L/CuSn10 multi-material bimetallic structure fabricated by selective laser melting. *Mater. Sci. Eng. A* 752, 75–85. doi:10.1016/j.msea.2019.02.097

Chen, K., Wang, C., Hong, Q., Wen, S., Zhou, Y., Yan, C., et al. (2020b). Selective laser melting 316L/CuSn10 multi-materials: Processing optimization, interfacial characterization and mechanical property. *J. Mater. Process. Technol.* 283, 116701. doi:10.1016/j.jmatprotec.2020.116701

Chowdhury, S., Yadaiah, N., Prakash, C., Ramakrishna, S., Dixit, S., Gupta, L. R., et al. (2022). Laser powder bed fusion: A state-of-the-art review of the technology, materials, properties & defects, and numerical modelling. *J. Mater. Res. Technol.* 20, 2109–2172. doi:10.1016/j.jmrt.2022.07.121

DebRoy, T., Wei, H. L., Zuback, J. S., Mukherjee, T., Elmer, J. W., Milewski, J. O., et al. (2018). Additive manufacturing of metallic components – process, structure and properties. *Prog. Mater. Sci.* 92, 112–224. doi:10.1016/j.pmatsci.2017.10.001

Demir, A. G., and Previtali, B. (2017). Multi-material selective laser melting of Fe/Al-12Si components. *Manuf. Lett.* 11, 8–11. doi:10.1016/j.mfglet.2017.01.002

Duval-Chaneac, M. S., Gao, N., Khan, R. H. U., Giles, M., Georgilas, K., Zhao, X., et al. (2021). Fatigue crack growth in IN718/316L multi-materials layered structures fabricated by laser powder bed fusion. *Int. J. Fatigue* 152, 106454. doi:10.1016/j.ijfatigue.2021.106454

Elton, E. S., Wu, Z., Troksa, M., and Guss, G. (2023). Electrostatic powder spreading for metal powder bed fusion applications. *Addit. Manuf.* 61, 103330. doi:10.1016/j.addma.2022.103330

Estrin, Y., Beygelzimer, Y., Kulagin, R., Gumbsch, P., Fratzl, P., Zhu, Y., et al. (2021). Architecturing materials at mesoscale: Some current trends. *Mater. Res. Lett.* 9, 399–421. doi:10.1080/21663831.2021.1961908

Fang, Y., Jiang, X., Mo, D., Zhu, D., and Luo, Z. (2019). A review on dissimilar metals' welding methods and mechanisms with interlayer. *Int. J. Adv. Manuf. Technol.* 102, 2845–2863. doi:10.1007/s00170-019-03353-6

Foerster, J., Michatz, M., Binder, M., Frey, A., Seidel, C., Schlick, G., et al. (2022a). Electrostatic powder attraction for the development of a novel recoating system for metal powder bed-based additive manufacturing. *J. Electrost.* 115, 103641. doi:10.1016/j.elstat.2021.103641

Foerster, J., Vranjes, K., Binder, M., Schlick, G., Seidel, C., and Schilp, J. (2022b). Electrophotographic powder application for metal powder bed based additive manufacturing. *Procedia CIRP* 113, 353–360. doi:10.1016/j.procir.2022.09.142

Foteinopoulos, P., Papacharalampopoulos, A., Angelopoulos, K., and Stavropoulos, P. (2020). Development of a simulation approach for laser powder bed fusion based on scanning strategy selection. *Int. J. Adv. Manuf. Technol.* 108, 3085–3100. doi:10.1007/s00170-020-05603-4

Furton, E. T., Wilson-Heid, A. E., and Beese, A. M. (2021). Effect of stress triaxiality and penny-shaped pores on tensile properties of laser powder bed fusion Ti-6Al-4V. *Addit. Manuf.* 48, 102414. doi:10.1016/j.addma.2021.102414

Galvele, J. R. (1987). A stress corrosion cracking mechanism based on surface mobility. *Corros. Sci.* 27, 1–33. doi:10.1016/0010-938X(87)90117-X

Garcia, D., Jones, M. E., Zhu, Y., and Yu, H. Z. (2018). Mesoscale design of heterogeneous material systems in multi-material additive manufacturing. *J. Mater. Res.* 33, 58–67. doi:10.1557/jmr.2017.328

Ge, W., Lin, F., and Guo, C. (2015). Functional gradient material of Ti-6Al-4V and γ-TiAl fabricated by electron beam selective melting. *2015 Int. Solid Free. Fabr. Symp.*, Available at: https://repositories.lib.utexas.edu/handle/2152/89362 (Accessed June 9, 2023).

Gene, M. (2022). Bend testing. Available at: https://www.twi-global.com/technical-knowledge/job-knowledge/bend-testing-073.aspx (Accessed October 10, 2022).

Ghanavati, R., and Naffakh-Moosavy, H. (2021). Additive manufacturing of functionally graded metallic materials: A review of experimental and numerical studies. *J. Mater. Res. Technol.* 13, 1628–1664. doi:10.1016/j.jmrt.2021.05.022

Girnth, S., Koopmann, J., Klawitter, G., Waldt, N., and Niendorf, T. (2019). 3D hybrid-material processing in selective laser melting: Implementation of a selective coating system. *Prog. Addit. Manuf.* 4, 399–409. doi:10.1007/s40964-019-00082-w

Gu, H., Wei, C., Li, L., Ryan, M., Setchi, R., Han, Q., et al. (2021). Numerical and experimental study of molten pool behaviour and defect formation in multi-material and functionally graded materials laser powder bed fusion. *Adv. Powder Technol.* 32, 4303–4321. doi:10.1016/j.apt.2021.09.036

Hasanov, S., Alkunte, S., Rajeshirke, M., Gupta, A., Huseynov, O., Fidan, I., et al. (2022). Review on additive manufacturing of multi-material parts: Progress and challenges. *J. Manuf. Mater. Process.* 6, 4. doi:10.3390/jmmp6010004

Hinojos, A., Mireles, J., Reichardt, A., Frigola, P., Hosemann, P., Murr, L. E., et al. (2016). Joining of Inconel 718 and 316 Stainless Steel using electron beam melting additive manufacturing technology. *Mater. Des.* 94, 17–27. doi:10.1016/j.matdes.2016.01.041

ISO/ASTM 52915 (2020). *Specification for additive manufacturing file format (AMF) version 1.2*.

Krishnaja, D., Cheepu, M., and Venkateswarlu, D. (2018). A review of research progress on dissimilar laser weld-brazing of automotive applications. *IOP Conf. Ser. Mater. Sci. Eng.* 330, 012073. doi:10.1088/1757-899X/330/1/012073

Lee, S. H. (2019). A hot cracking on dissimilar metal weld between A106Gr.B and A312 TP316L with buttering ERNiCr-3. *Metals* 9, 533. doi:10.3390/met9050533

Li, E., Zhou, Z., Wang, L., Zou, R., and Yu, A. (2022). Particle scale modelling of powder recoating and melt pool dynamics in laser powder bed fusion additive manufacturing: A review. *Powder Technol.* 409, 117789. doi:10.1016/j.powtec.2022.117789

Li, Y., Feng, Z., Hao, L., Huang, L., Xin, C., Wang, Y., et al. (2020). A review on functionally graded materials and structures via additive manufacturing: From multi-scale design to versatile functional properties. *Adv. Mater. Technol.* 5, 1900981. doi:10.1002/admt.201900981

Liu, Y., Wang, Y., Wu, X., and Shi, J. (2020). Nonequilibrium thermodynamic calculation and experimental investigation of an additively manufactured functionally graded material. *J. Alloys Compd.* 838, 155322. doi:10.1016/j.jallcom.2020.155322

Liu, Z. H., Zhang, D. Q., Sing, S. L., Chua, C. K., and Loh, L. E. (2014). Interfacial characterization of SLM parts in multi-material processing: Metallurgical diffusion between 316L stainless steel and C18400 copper alloy. *Mater. Charact.* 94, 116–125. doi:10.1016/j.matchar.2014.05.001

Luo, Q., Yin, L., Simpson, T. W., and Beese, A. M. (2022). Effect of processing parameters on pore structures, grain features, and mechanical properties in Ti-6Al-4V by laser powder bed fusion. *Addit. Manuf.* 56, 102915. doi:10.1016/j.addma.2022.102915

Marques, A., Cunha, Â., Gasik, M., Carvalho, O., Silva, F. S., and Bartolomeu, F. (2022). Inconel 718–copper parts fabricated by 3D multi-material laser powder bed fusion: A novel technological and designing approach for rocket engine. *Int. J. Adv. Manuf. Technol.* 122, 2113–2123. doi:10.1007/s00170-022-10011-x

Martin, A. A., Calta, N. P., Khairallah, S. A., Wang, J., Depond, P. J., Fong, A. Y., et al. (2019). Dynamics of pore formation during laser powder bed fusion additive manufacturing. *Nat. Commun.* 10, 1987. doi:10.1038/s41467-019-10009-2

Mei, X., Wang, X., Peng, Y., Gu, H., Zhong, G., and Yang, S. (2019). Interfacial characterization and mechanical properties of 316L stainless steel/inconel 718 manufactured by selective laser melting. *Mater. Sci. Eng. A* 758, 185–191. doi:10.1016/j.msea.2019.05.011

Mo, D., Song, T., Fang, Y., Jiang, X., Luo, C. Q., Simpson, M. D., et al. (2018). A review on diffusion bonding between titanium alloys and stainless steels. *Adv. Mater. Sci. Eng.* 2018, 1–15. doi:10.1155/2018/8701890

Mostafaei, A., Zhao, C., He, Y., Reza Ghiaasiaan, S., Shi, B., Shao, S., et al. (2022). Defects and anomalies in powder bed fusion metal additive manufacturing. *Curr. Opin. Solid State Mater. Sci.* 26, 100974. doi:10.1016/j.cossms.2021.100974

Moustafa, A. R., Durga, A., Lindwall, G., and Cordero, Z. C. (2020). Scheil ternary projection (STeP) diagrams for designing additively manufactured functionally graded metals. *Addit. Manuf.* 32, 101008. doi:10.1016/j.addma.2019.101008

Mukherjee, T., Zuback, J. S., Zhang, W., and DebRoy, T. (2018). Residual stresses and distortion in additively manufactured compositionally graded and dissimilar joints. *Comput. Mater. Sci.* 143, 325–337. doi:10.1016/j.commatsci.2017.11.026

Nadimpalli, V. K., Dahmen, T., Valente, E. H., Mohanty, S., and Pedersen, D. B. (2019). Multi-material additive manufacturing of steels using laser powder bed fusion. *Proc. 19th Int. Conf. Exhib. (EUSPEN 2019)*, 240–243.

Naebe, M., and Shirvanimoghaddam, K. (2016). Functionally graded materials: A review of fabrication and properties. *Appl. Mater. Today* 5, 223–245. doi:10.1016/j.apmt.2016.10.001

Nguyen, D.-S., Park, H.-S., and Lee, C.-M. (2019). Applying selective laser melting to join Al and Fe: An investigation of dissimilar materials. *Appl. Sci.* 9, 3031. doi:10.3390/app9153031

Peters, M., Kumpfert, J., Ward, C. h., and Leyens, C. (2003). Titanium alloys for aerospace applications. *Adv. Eng. Mater.* 5, 419–427. doi:10.1002/adem.200310095

Rankouhi, B., Islam, Z., Pfefferkorn, F. E., and Thoma, D. J. (2022). Characterization of multi-material 316L-Hastelloy X fabricated via laser powder-bed fusion. *Mater. Sci. Eng. A* 837, 142749. doi:10.1016/j.msea.2022.142749

Raut, L. P., and Taiwade, R. V. (2021). Wire arc additive manufacturing: A comprehensive review and research directions. *J. Mater. Eng. Perform.* 30, 4768–4791. doi:10.1007/s11665-021-05871-5

Rossini, M., Spena, P. R., Cortese, L., Matteis, P., and Firrao, D. (2015). Investigation on dissimilar laser welding of advanced high strength steel sheets for the automotive industry. *Mater. Sci. Eng. A* 628, 288–296. doi:10.1016/j.msea.2015.01.037

Sanchez, S., Gaspard, G., Hyde, C. J., Ashcroft, I. A., and Clare, A. T. (2021). The creep behaviour of nickel alloy 718 manufactured by laser powder bed fusion. *Mater. Des.* 204, 109647. doi:10.1016/j.matdes.2021.109647

Scaramuccia, M. G., Demir, A. G., Caprio, L., Tassa, O., and Previtali, B. (2020). Development of processing strategies for multigraded selective laser melting of Ti6Al4V and IN718. *Powder Technol.* 367, 376–389. doi:10.1016/j.powtec.2020.04.010

Schneck, M., Horn, M., Schmitt, M., Seidel, C., Schlick, G., and Reinhart, G. (2021). Review on additive hybrid- and multi-material-manufacturing of metals by powder bed fusion: State of technology and development potential. *Prog. Addit. Manuf.* 6, 881–894. doi:10.1007/s40964-021-00205-2

Shunmugavel, M., Polishetty, A., and Littlefair, G. (2015). Microstructure and mechanical properties of wrought and additive manufactured Ti-6Al-4V cylindrical bars. *Procedia Technol.* 20, 231–236. doi:10.1016/j.protcy.2015.07.037

Sing, S. L., Lam, L. P., Zhang, D. Q., Liu, Z. H., and Chua, C. K. (2015). Interfacial characterization of SLM parts in multi-material processing: Intermetallic phase formation between AlSi10Mg and C18400 copper alloy. *Mater. Charact.* 107, 220–227. doi:10.1016/j.matchar.2015.07.007

Stavropoulos, P., and Foteinopoulos, P. (2018). Modelling of additive manufacturing processes: A review and classification. *Manuf. Rev.* 5, 2. doi:10.1051/mfreview/2017014

Sun, Z., Chueh, Y.-H., and Li, L. (2020). Multiphase mesoscopic simulation of multiple and functionally gradient materials laser powder bed fusion additive manufacturing processes. *Addit. Manuf.* 35, 101448. doi:10.1016/j.addma.2020.101448

Sun, Z., Tan, X., Tor, S. B., and Yeong, W. Y. (2016). Selective laser melting of stainless steel 316L with low porosity and high build rates. *Mater. Des.* 104, 197–204. doi:10.1016/j.matdes.2016.05.035

Svetlizky, D., Das, M., Zheng, B., Vyatskikh, A. L., Bose, S., Bandyopadhyay, A., et al. (2021). Directed energy deposition (DED) additive manufacturing: Physical characteristics, defects, challenges and applications. *Mater. Today* 49, 271–295. doi:10.1016/j.mattod.2021.03.020

Tan, C., Zhou, K., and Kuang, T. (2019). Selective laser melting of tungsten-copper functionally graded material. *Mater. Lett.* 237, 328–331. doi:10.1016/j.matlet.2018.11.127

Tan, C., Zhou, K., Ma, W., and Min, L. (2018). Interfacial characteristic and mechanical performance of maraging steel-copper functional bimetal produced by selective laser melting based hybrid manufacture. *Mater. Des.* 155, 77–85. doi:10.1016/j.matdes.2018.05.064

Taylor, N., Faidy, C., and Gilles, P. (Editors) (2006). (European Commission Joint Research Centre). Available at: https://op.europa.eu/en/publication-detail/-/publication/3483d8df-981b-477e-80e6-07f77927e953.*Assessment of weld integrity: Final report of the NESC-III project*.

Tey, C. F., Tan, X., Sing, S. L., and Yeong, W. Y. (2020). Additive manufacturing of multiple materials by selective laser melting: Ti-Alloy to stainless steel via a Cu-alloy interlayer. *Addit. Manuf.* 31, 100970. doi:10.1016/j.addma.2019.100970

Vafadar, A., Guzzomi, F., Rassau, A., and Hayward, K. (2021). Advances in metal additive manufacturing: A review of common processes, industrial applications, and current challenges. *Appl. Sci.* 11, 1213. doi:10.3390/app11031213

Vialva, T. (2019). Aerosint and Aconity3D collaborate to accelerate laser powder bed fusion additive manufacturing. *3D Print. Ind.*, Available at: https://3dprintingindustry.com/news/aerosint-and-aconity3d-collaborate-to-accelerate-laser-powder-bed-fusion-additive-manufacturing-149406/(Accessed October 4, 2022).

Walker, J., Middendorf, J. R., Lesko, C. C. C., and Gockel, J. (2022). Multi-material laser powder bed fusion additive manufacturing in 3-dimensions. *Manuf. Lett.* 31, 74–77. doi:10.1016/j.mfglet.2021.07.011

Wang, D., Deng, G., Yang, Y., Chen, J., Wu, W., Wang, H., et al. (2021). Interface microstructure and mechanical properties of selective laser melted multilayer functionally graded materials. *J. Central South Univ.* 28, 1155–1169. doi:10.1007/s11771-021-4687-9

Wang, P., Chen, X., Pan, Q., Madigan, B., and Long, J. (2016). Laser welding dissimilar materials of aluminum to steel: An overview. *Int. J. Adv. Manuf. Technol.* 87, 3081–3090. doi:10.1007/s00170-016-8725-y

Wang, P., Lao, C. S., Chen, Z. W., Liu, Y. K., Wang, H., Wendrock, H., et al. (2020). Microstructure and mechanical properties of Al-12Si and Al-3.5Cu-1.5Mg-1Si bimetal fabricated by selective laser melting. *J. Mater. Sci. Technol.* 36, 18–26. doi:10.1016/j.jmst.2019.03.047

Wei, C., Gu, H., Li, Q., Sun, Z., Chueh, Y., Liu, Z., et al. (2021). Understanding of process and material behaviours in additive manufacturing of Invar36/Cu10Sn multiple material components via laser-based powder bed fusion. *Addit. Manuf.* 37, 101683. doi:10.1016/j.addma.2020.101683

Wei, C., Gu, H., Sun, Z., Cheng, D., Chueh, Y.-H., Zhang, X., et al. (2019a). Ultrasonic material dispensing-based selective laser melting for 3D printing of metallic components and the effect of powder compression. *Addit. Manuf.* 29, 100818. doi:10.1016/j.addma.2019.100818

Wei, C., and Li, L. (2021). Recent progress and scientific challenges in multi-material additive manufacturing via laser-based powder bed fusion. *Virtual Phys. Prototyp.* 16, 347–371. doi:10.1080/17452759.2021.1928520

Wei, C., Li, L., Zhang, X., and Chueh, Y.-H. (2018). 3D printing of multiple metallic materials via modified selective laser melting. *CIRP Ann.* 67, 245–248. doi:10.1016/j.cirp.2018.04.096

Wei, C., Liu, L., Gu, Y., Huang, Y., Chen, Q., Li, Z., et al. (2022). Multi-material additive-manufacturing of tungsten - copper alloy bimetallic structure with a stainless-steel interlayer and associated bonding mechanisms. *Addit. Manuf.* 50, 102574. doi:10.1016/j.addma.2021.102574

Wei, C., Sun, Z., Chen, Q., Liu, Z., and Li, L. (2019b). Additive manufacturing of horizontal and 3D functionally graded 316L/Cu10Sn components via multiple material selective laser melting. *J. Manuf. Sci. Eng.* 141. doi:10.1115/1.4043983

Wei, K., Zeng, X., Li, F., Liu, M., and Deng, J. (2020). Microstructure and mechanical property of Ti-5Al-2.5Sn/Ti-6Al-4V dissimilar titanium alloys integrally fabricated by selective laser melting. *JOM* 72, 1031–1038. doi:10.1007/s11837-019-03988-6

Weigl, J. W. (1977). Electrophotography. *Angewandte Chemie Int. Ed. Engl.* 16, 374–392. doi:10.1002/anie.197703741

Wilson-Heid, A. E., Novak, T. C., and Beese, A. M. (2019). Characterization of the effects of internal pores on tensile properties of additively manufactured austenitic stainless steel 316L. *Exp. Mech.* 59, 793–804. doi:10.1007/s11340-018-00465-0

Xin, J., Zhang, H., Sun, W., Huang, C., Wang, S., Wei, J., et al. (2021). The microstructures and mechanical properties of dissimilar laser welding of copper and 316L stainless steel with Ni interlayer. *Cryogenics* 118, 103344. doi:10.1016/j.cryogenics.2021.103344

Yu, H. Z., Cross, S. R., and Schuh, C. A. (2017). Mesostructure optimization in multi-material additive manufacturing: A theoretical perspective. *J. Mater. Sci.* 52, 4288–4298. doi:10.1007/s10853-017-0753-y

Yusuf, S. M., Zhao, X., Yang, S., and Gao, N. (2021). Interfacial characterisation of multi-material 316L stainless steel/Inconel 718 fabricated by laser powder bed fusion. *Mater. Lett.* 284, 128928. doi:10.1016/j.matlet.2020.128928

Zhang, J., Song, B., Yang, L., Liu, R., Zhang, L., and Shi, Y. (2020). Microstructure evolution and mechanical properties of TiB/Ti6Al4V gradient-material lattice structure fabricated by laser powder bed fusion. *Compos. Part B Eng.* 202, 108417. doi:10.1016/j.compositesb.2020.108417

Zhang, M., Yang, Y., Wang, D., Song, C., and Chen, J. (2019). Microstructure and mechanical properties of CuSn/18Ni300 bimetallic porous structures manufactured by selective laser melting. *Mater. Des.* 165, 107583. doi:10.1016/j.matdes.2019.107583